The EGR2 targets LAG-3 and 4-1BB describe and regulate dysfunctional antigen-specific CD8$^+$ T cells in the tumor microenvironment

Jason B. Williams,[1] Brendan L. Horton,[1] Yan Zheng,[1] Yukan Duan,[3] Jonathan D. Powell,[4] and Thomas F. Gajewski[1,2]

[1]Departments of Pathology, Section of Hematology/Oncology, the University of Chicago, Chicago, IL 60637
[2]Department of Medicine, Section of Hematology/Oncology, the University of Chicago, Chicago, IL 60637
[3]Department of Ophthalmology, Johns Hopkins University School of Medicine, Baltimore, MD 21287
[4]Sidney Kimmel Comprehensive Cancer Research Center, Department of Oncology, Johns Hopkins University School of Medicine, Baltimore, MD 21231

Although the presence of tumor-infiltrating lymphocytes (TILs) indicates an endogenous antitumor response, immune regulatory pathways can subvert the effector phase and enable tumor escape. Negative regulatory pathways include extrinsic suppression mechanisms, but also a T cell–intrinsic dysfunctional state. A more detailed study has been hampered by a lack of cell surface markers defining tumor-specific dysfunctional TILs, and PD-1 alone is not sufficient. Recently, we identified the transcription factor Egr2 as a critical component in controlling the anergic state in vitro. In this study, we show that the Egr2-driven cell surface proteins LAG-3 and 4-1BB can identify dysfunctional tumor antigen–specific CD8$^+$ TIL. Co-expression of 4-1BB and LAG-3 was seen on a majority of CD8$^+$ TILs, but not in lymphoid organs. Functional analysis revealed defective IL-2 and TNF production yet retained expression of IFN-γ and regulatory T cell–recruiting chemokines. Transcriptional and phenotypic characterization revealed coexpression of multiple additional co-stimulatory and co-inhibitory receptors. Administration of anti–LAG-3 plus anti–4-1BB mAbs was therapeutic against tumors in vivo, which correlated with phenotypic normalization. Our results indicate that coexpression of LAG-3 and 4-1BB characterize dysfunctional T cells within tumors, and that targeting these receptors has therapeutic utility.

INTRODUCTION

The immune system can play a critical role in protecting the host from cancer (Vesely et al., 2011). Innate sensing of tumors can lead to an adaptive T cell response through the presentation of tumor-associated antigens (TAAs) derived from mutations and epigenetic changes that contribute to carcinogenesis (Gajewski et al., 2013). Spontaneously primed CD8$^+$ T cells can home to tumor sites in mouse tumor models (Harlin et al., 2009; Fuertes et al., 2011) and in a subset of patients with advanced cancer (Harlin et al., 2006). These tumor-infiltrating lymphocytes (TILs) have the ability to recognize tumor antigens and are believed to contribute to tumor control in cancer patients, based on the correlation between activated CD8$^+$ T cell infiltration with improved prognosis and response to immunotherapy (Fridman et al., 2012; Tumeh et al., 2014). However, without additional manipulation, this endogenous anti-tumor response is usually not sufficient to mediate complete rejection of an established tumor (Gajewski et al., 2006, 2007b; Baitsch et al., 2011; Pardoll, 2012; Larkin et al., 2015). Data accumulated over the past several years have indicated that tumors with spontaneous antitumor T cell responses have high expression of immune-inhibitory pathways that subvert the effector phase of the response. These include PD-L1–PD-1 interactions (Pardoll, 2012), recruitment of CD4$^+$Foxp3$^+$ regulatory T (T reg) cells (Gajewski, 2007a), and metabolic dysregulation by indoleamine-2,3-dioxygenase (IDO; Spranger et al., 2013). However, even when CD8$^+$ T cells specific for tumor antigens are isolated from tumors, away from these extrinsic immune inhibitory factors, they still show altered functional properties ex vivo (Harlin et al., 2006; Baitsch et al., 2011). This latter observation suggests that there are T cell–intrinsic mechanisms that contribute to failed de novo immune-mediated tumor rejection. A deeper understanding of this putative T cell–intrinsic defect should lead to further improvements of immunotherapies aimed at restoring the function of those T cells to ultimately support tumor rejection (Gajewski, 2007b).

Much of the work done dissecting CD8$^+$ T cell dysfunction in the tumor microenvironment has been translated from

Correspondence to Thomas F. Gajewski: tgajewsk@medicine.bsd.uchicago.edu

Abbreviations used: CTLA, cytotoxic T lymphocyte–associated protein; HD, Hamming distance; IDO, indoleamine-2,3-dioxygenase; TAA, tumor-associated antigen; TDLN, tumor-draining lymph node; TIGIT, T cell immunoreceptor with Ig and ITIM domain; TIL, tumor infiltrating lymphocyte; .

The Rockefeller University Press $30.00
J. Exp. Med. 2017 Vol. 214 No. 2 381–400
https://doi.org/10.1084/jem.20160485

chronic infection examples, such as the chronic LCMV mouse model (Pauken and Wherry, 2015). In particular, expression of PD-1 has been described to identify tumor-specific exhausted T cells (Ahmadzadeh et al., 2009; Fourcade et al., 2012; Gros et al., 2014; Wu et al., 2014). However, it is becoming clear that T cells expressing PD-1 in the context of chronic infection can still retain effector function (Wherry and Kurachi, 2015), and that PD-1 is not required for the induction of T cell exhaustion (Odorizzi et al., 2015). In addition to PD-1, several additional co-inhibitory receptors, including CD223 (LAG-3), CD244 (2B4), T cell immunoreceptor with Ig and ITIM domains (TIGIT), hepatitis A virus cellular receptor 2 (TIM-3), and cytotoxic T lymphocyte–associated protein 4 (CTLA-4), can also be expressed on dysfunctional T cells, and expression of a greater number of inhibitory receptors has been correlated with diminished cytokine secretion (particularly IFN-γ and TNF), as well as proliferative capacity (Blackburn et al., 2009). Expression of these receptors has been observed in both viral and cancer models, however, a complete analysis of both co-inhibitory and co-stimulatory receptors on the same population is lacking in the tumor setting. Similarities between viral chronic infections and solid tumors, such as the persistence of antigen, do exist. However, the metabolic provisions and demands on the immune response, the anatomical localization of the process, and the cellular components involved in these two chronic diseases are disparate enough to warrant further direct investigation into T cell dysfunction within the tumor environment as a specific tissue context.

Recently, we identified the transcription factor Egr2 as a critical regulator of the anergic state in $CD4^+$ T cell clones manipulated in vitro (Zheng et al., 2012, 2013). Egr2 has also been shown to be involved in negative regulation of T cell activation in several in vivo model systems (Sumitomo et al., 2013). Egr2 contributes to up-regulation of DGK-α and -ζ which act to blunt TCR-mediated Ras pathway activation (Zha et al., 2006). By comparing gene expression profiling of anergized cells along with Egr2 ChIP-Seq analysis, we identified multiple additional Egr2-driven gene targets (Zheng et al., 2013). These gene targets include *Tnfrsf9*, *Lag3*, *Nrn1*, *Sema7a*, *Crtam*, and *Rankl*, which encode cell surface proteins. We reasoned that expression of these and other Egr2 targets may have the potential to identify a global state of T cell differentiation associated with T cell dysfunction in vivo.

Tnfrsf9 (4-1BB or CD137) is a co-stimulatory molecule transiently expressed after TCR engagement. *Lag3* (lymphocyte-activation gene 3 or CD223) is a CD4 homologue and functions as an inhibitory receptor. Expression of *Tnfrsf9* and *Lag3* is regulated after TCR engagement and continues throughout differentiation. In humans, 4-1BB and LAG-3 can be expressed on $CD8^+$ TILs from melanoma tumors (Baitsch et al., 2012; Gros et al., 2014). In both mice and humans, either molecule alone can be expressed on activated T cells. However, coexpression is more limited and is rarely observed in circulating T cells. The function of $CD8^+$ TILs coexpressing these markers is unknown.

In this study, based on the hypothesis that coexpression of 4-1BB and LAG-3 might define dysfunctional T cells in the tumor context, we investigated the detailed characteristics of $CD8^+$ TILs expressing 4-1BB and LAG-3 using mouse tumor models. We found that the coexpression of 4-1BB and LAG-3 was sufficient to identify tumor antigen–specific dysfunctional $CD8^+$ TILs enriched in the expression of Egr2 target genes. These $CD8^+$ TILs failed to make IL-2 after in vitro stimulation, yet still produced IFN-γ and T reg cell–recruiting chemokines and lysed target cells ex vivo, arguing they are not completely functionally inert. Combinatorial treatment with anti–LAG-3/anti–4-1BB restored the function of this population and promoted in situ acquisition of KLRG-1^{hi} effector cells. Additional gene expression profiling provided a complete phenotyping of this T cell subset, which revealed expression of a broad panel of both inhibitory receptors and co-stimulatory receptors. These approaches have thus enabled the characterization of the population of tumor antigen–specific $CD8^+$ T cells that arise specifically within the tumor microenvironment having altered functional properties, and have highlighted targets for novel immunotherapeutic approaches to restore desired functionality and promote tumor regression.

RESULTS

4-1BB and LAG-3 identify a major population of $CD8^+$ TILs

To determine whether 4-1BB and LAG-3 could identify dysfunctional $CD8^+$ TILs, we examined the expression pattern of LAG-3 and 4-1BB using the well-characterized B16.SIY model of melanoma. On day 7 after tumor inoculation, the 4-$1BB^+$LAG-3^+ population comprised 15.8% of all $CD8^+$ TILs. The frequency of this population significantly increased to 44% by day 21. The frequency of 4-$1BB^-$LAG-3^+ (4^-L^+) population also increased 1.9-fold from day 7 to day 14 to comprise 25% of the $CD8^+$ TIL compartment. In contrast, the frequency of the 4-$1BB^-$LAG-3^- (4^-L^-) population decreased by 2.7-fold by day 21. As there was no significant increase in the proportion or number of 4-$1BB^+$LAG-3^- $CD8^+$ TILs within the time frame of the experiment (Fig. 1, A and B), this population was not studied further. Similar patterns were seen when analyzing absolute numbers of cell subsets (Fig. 1, C and D). Acquisition of these phenotypes was specific for the tumor microenvironment, as they were not observed in the spleen or tumor-draining lymph node (TdLN; Fig. 1 A). These data suggest that the tumor microenvironment preferentially supports the induced coexpression of LAG-3 and 4-1BB.

The selective increase in cell numbers and proportional shift toward the 4-$1BB^-$LAG-3^+ and 4-$1BB^+$LAG-3^+ populations during tumor progression suggested that expansion of these populations was occurring within the tumor microenvironment. To investigate this possibility, $CD8^+$ TILs were stained for Ki67 at day 14 after tumor inoculation and analyzed by flow cytometry. In fact, 81% of 4-$1BB^-$LAG-3^+ cells and 85% of 4-$1BB^+$LAG-3^+ cells were $Ki67^+$ compared with

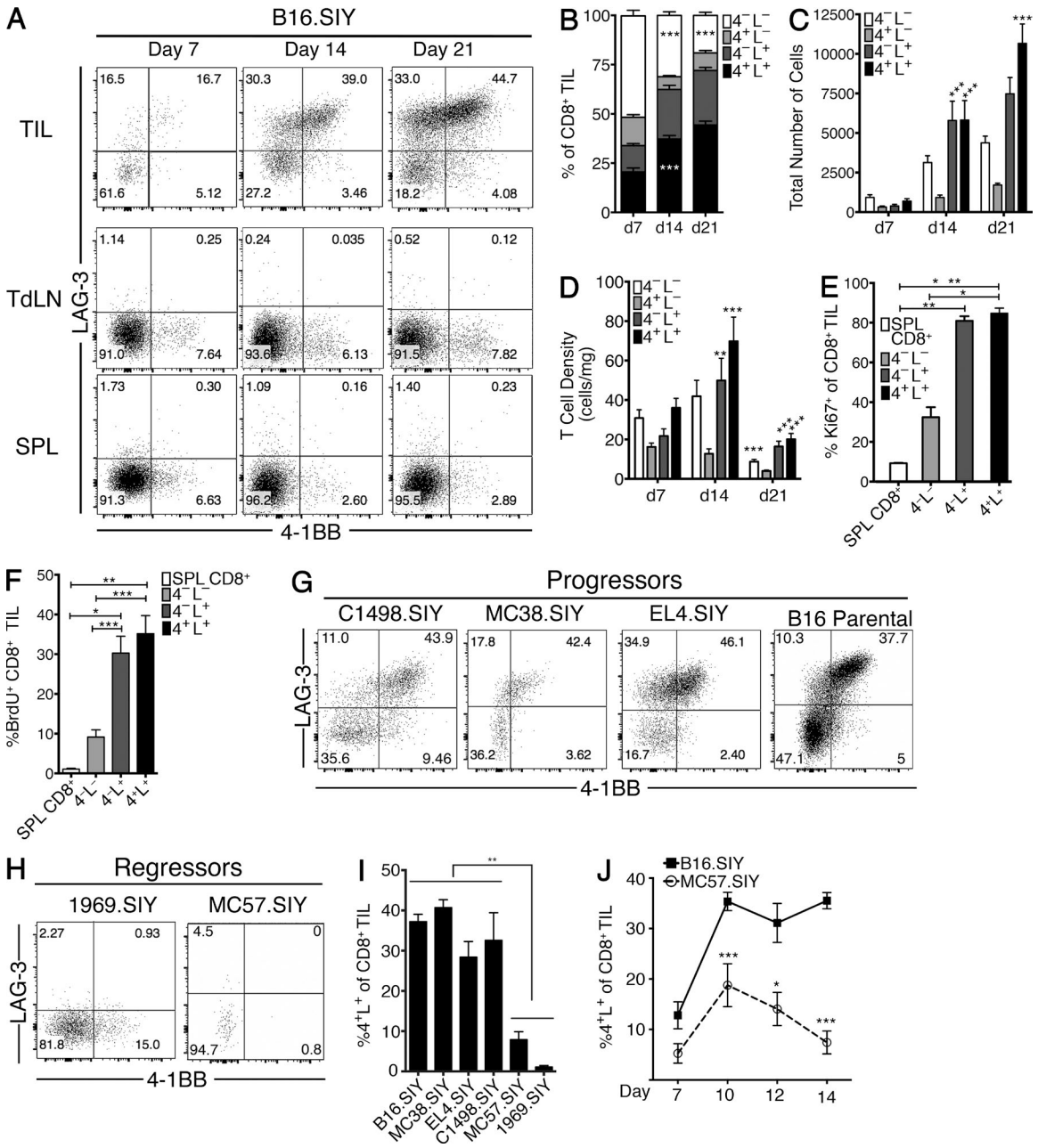

Figure 1. **Co-expression of 4-1BB and LAG-3 identifies a significant fraction of the CD8+ TIL compartment found in progressing tumors.** (A) Representative analysis of 4-1BB and LAG-3 expression on CD8+ T cells from B16.SIY tumors and the spleen and TdLN from tumor bearing mice on day 7, 14 and 21 after s.c. tumor inoculation. (B–D) Longitudinal summary of the composition, $n = 5$; four to five independent experiments per time point, (C) absolute cell number, $n = 5$; seven to nine independent experiments per time point, and (D) cellular density of the CD8+ 4-1BB/LAG-3 TIL subpopulations, $n = 5$; two to five independent experiments per time point. Absolute cell numbers were estimated by acquiring the complete tumor sample by flow cytometry. (E) Day 14 summary of the proportion of the CD8+ 4-1BB/LAG-3 TIL subpopulations that are Ki67+. $n = 3$–5; two independent experiments. (F) Summary of BrdU uptake on day 13 in the CD8+ 4-1BB/LAG-3 TIL subpopulations after a 24-h BrdU pulse. $n = 5$; three independent experiments. (G–I) Representative flow plots (G and H) and summary (I) of the 4-1BB/LAG-3 populations in other tumor models. Mice were inoculated with 2×10^6 C1498.SIY, MC38.SIY, EL4.SIY, B16 Parental, MC57.SIY, or 1969.SIY s.c. and analyzed for 4-1BB and LAG-3 expression on day 14 after tumor inoculation. $n = 3$–5; two to five independent experiments for each time point. (J) Mice were inoculated on both flanks with 2×10^6 MC57.SIY or B16.SIY at indicated time points tumors from each mouse were pooled and analyzed for coexpression of 4-1BB and LAG-3 in the CD8+ TIL compartment. $n = 3$–5; two independent experiments for each time point. All error bars indicate mean ± SEM. *, $P < 0.05$; **, $P < 0.01$; ***, $P < 0.001$. A two-way ANOVA with Bonferroni post-hoc test was used for longitudinal studies (B–D and H) and Kruskal-Wallis (nonparametric) test was used for analysis at one time point (E and F).

only 32% of the 4-1BB$^-$LAG-3$^-$ TILs (Fig. 1 E). To further investigate this process, mice were pulsed with BrdU on day 12 and, 24 h later, the CD8$^+$ TIL subpopulations were analyzed for BrdU incorporation. Indeed, the 4-1BB$^-$LAG-3$^+$ and 4-1BB$^+$LAG-3$^+$ populations incorporated more BrdU compared with the 4-1BB$^-$LAG-3$^-$ population (Fig. 1 F). These data suggest that once CD8$^+$ T cells arrive at the tumor site, a fraction of TILs expands within the tumor, and that these expanding TILs can be identified by increased expression of 4-1BB and LAG-3.

To determine if up-regulation of LAG-3 and 4-1BB was simply a product of the B16.SIY tumor model or if it is a more general feature of CD8$^+$ T cells within tumors, we analyzed T cells from three additional progressively growing tumor models, C1498.SIY, MC38.SIY, EL4.SIY, and B16F10 parental. TILs were analyzed for expression of 4-1BB and LAG-3 at day 14. We found that the pattern of expression was similar to that seen in CD8$^+$ TILs isolated from B16.SIY tumors (Fig. 1, G and I). The results from the B16F10 parental tumor confirm that presence of SIY is not required to see coexpression of 4-1BB and LAG-3. To determine whether the 4-1BB$^+$LAG-3$^+$ TIL subset was generated only in progressing tumors or also in tumors that were rejected, we analyzed T cell phenotypes in the 1969.SIY and MC57.SIY fibrosarcoma tumor models, which are more immunogenic and undergo spontaneous rejection. Interestingly, distinctly fewer 4-1BB$^+$LAG-3$^+$ cells were found among the CD8$^+$ TIL compartment in the 1969.SIY and MC57.SIY tumors (Fig. 1, H and I). Over time, coexpression of 4-1BB and LAG-3 was maintained in B16.SIY tumors, but not MC57.SIY tumors (Fig. 1 J). These data suggest that the acquisition of the LAG-3$^+$4-1BB$^+$ TIL phenotype preferentially occurs within the tumor microenvironment and only upon conditions of tumor progression rather than regression.

CD8$^+$4-1BB$^+$LAG-3$^+$ TILs express Egr2 and multiple Egr2 gene targets

Based on previous studies describing Egr2 as a critical regulator of T cell activation in vitro and in vivo (Safford et al., 2005; Li et al., 2012; Sumitomo et al., 2013), and accompanied by our previous finding that Egr2 regulates the expression of 4-1BB and LAG-3 in an in vitro model of anergy (Zheng et al., 2013), we investigated whether Egr2 expression itself was also characteristic of T cells within the CD8$^+$ TIL compartment. To this end, we used an Egr2-IRES-GFP (Egr2^{GFP}) knock-in reporter mouse. Approximately 14% of all CD8$^+$ TILs were GFP$^+$ on both day 7 and 14 (Fig. 2 A). To confirm that Egr2 is faithfully reported we sorted CD8$^+$ TILs expressing high and low levels of EGFP and subsequently screened for Egr2 and several Egr2 targets by qRT-PCR. The Egr2-GFP^{hi} population expressed greater levels of Egr2 and many Egr2-target genes previously defined using in vitro anergy models. These include *Tnfrsf9*, *Lag3*, *Ngn*, *Sema7a*, *Crtam*, *Ccl1*, and *Nrn1* (Fig. 2 B). Expression of 4-1BB and LAG-3 in the Egr2-GFP^{hi} CD8$^+$ TILs was confirmed by flow cytometry. The majority of Egr2-GFP^{hi} cells expressed LAG-3 and/or 4-1BB. The Egr2GFP^{lo} cells also showed expression of 4-1BB and LAG-3 on a subpopulation at day 14 (Fig. 2 C). This result suggests either that CD8$^+$ TILs expressing Egr2 encompass only a subset of the TILs expressing LAG-3 and/or 4-1BB, or that Egr2 is transiently expressed and is subsequently down-regulated after the induction of LAG-3 and 4-1BB.

Using previously identified Egr2 target genes from in vitro anergic CD4$^+$ T cell clones (Zheng et al., 2013), we examined the Egr2-driven transcriptional program in sorted 4-1BB$^-$LAG-3$^-$ and 4-1BB$^+$LAG-3$^+$ cells by qRT-PCR. Of the 43 Egr2 target genes examined, 10 showed detectably increased expression in 4-1BB$^+$LAG-3$^+$ population (Fig. 2 D). Collectively, these data show that Egr2 is expressed in a subpopulation of CD8$^+$ TILs expressing LAG-3 and 4-1BB, and that a subset of known Egr2 targets was detected in these larger T cell populations as a whole.

We next examined whether Egr2 was required for expression of LAG-3 and 4-1BB among CD8$^+$ TIL in vivo. To this end, we used Egr2$^{flox/flox}$ X pLCK-CreERT2 x ROSA-YFP mice, in which oral tamoxifen administration results in a fraction of the CD8$^+$ T cells deleting Egr2 and expressing YFP (Fig. 2 E). This allowed us to compare both Egr2-sufficient (YFP$^-$) and Egr2-deficient (YFP$^+$) CD8$^+$ within the same tumor. To determine that Egr2 was in fact deleted from the YFP$^+$ fraction, we sorted both YFP$^+$ and YFP$^-$ CD8$^+$ TILs and measured *Egr2* transcripts directly ex vivo and upon ex vivo stimulation. As expected, the YFP$^+$ CD8$^+$ TILs expressed substantially less *Egr2* transcripts compared with the YFP$^-$ counterparts (Fig. 2 E). To determine if Egr2 is required for 4-1BB and LAG-3 expression, we analyzed CD8$^+$ TILs at day 7 and 14 after tumor inoculation and compared the YFP$^+$ and YFP$^-$ populations to mice not treated with tamoxifen. Indeed, at day 7, the YFP$^+$ fraction expressed less 4-1BB and LAG-3 compared with the YFP$^-$ population and the WT CD8$^+$ TILs. However, expression of 4-1BB and LAG-3 was not significantly different at day 14 (Fig. 2 F). This suggests that other transcriptional regulators may compensate and contribute to the expression of LAG-3 and 4-1BB, especially at later time points.

Egr3 has been shown to have overlapping function with Egr2 (Safford et al., 2005), and HIF1α can contribute to 4-1BB expression (Palazón et al., 2012). To investigate whether these transcription factors may compensate for 4-1BB and/or LAG-3 expression we sorted Egr2GFP^{hi} and Egr2GFP^{lo} CD8$^+$ TILs expressing 4-1BB and LAG-3 on day 7 and analyzed expression of *Egr3* and *HIF1α* by qRT-PCR. *Egr3* and *HIF1α* were indeed expressed in both the Egr2GFP^{hi} and Egr2GFP^{lo} populations. We confirmed differential expression of Egr2 and CCL1 between the Egr2GFP^{hi} and Egr2GFP^{lo} populations to assure sort purity (Fig. 2 G). Together, these data indicate that Egr2 contributes to up-regulation of 4-1BB and LAG-3 expression at early time points, but that other transcriptional regulators may compensate and drive expression of LAG-3 and 4-1BB as the T cell–tumor interaction progresses.

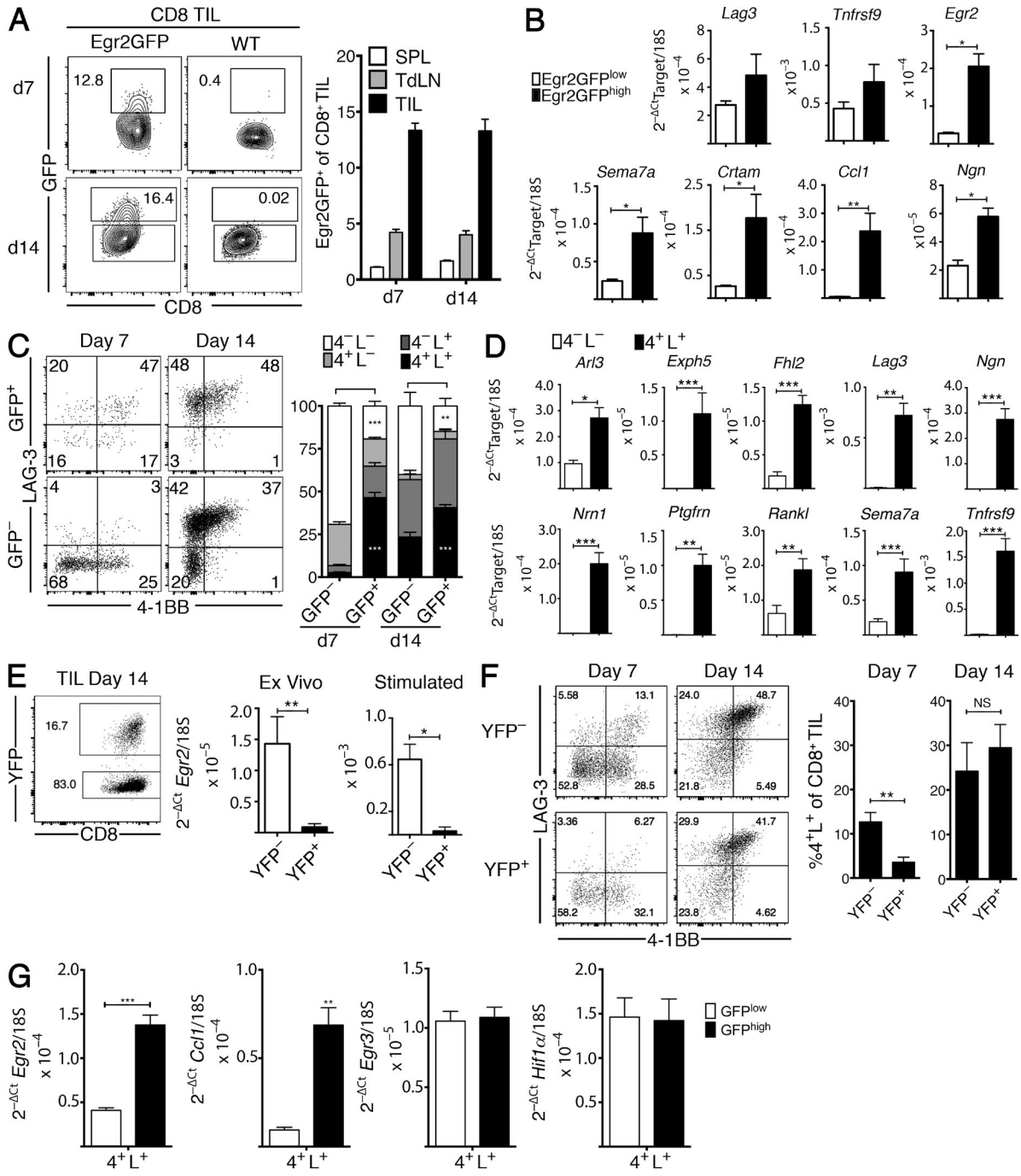

Figure 2. **Egr2 and a component of the Egr2-transcriptional network are enriched in 4-1BB$^+$LAG-3$^+$ CD8$^+$ TILs.** (A) Representative flow plot and summary of Egr2^{EGFP} expression. Egr2^{EGFP} mice were inoculated with 2 × 10^6 B16.SIY tumors s.c. CD8$^+$ T cells from the tumor, TdLN, and spleen were analyzed for Egr2^{EGFP} expression on day 7 and 14. *n* = 4–5; two independent experiments. (B) Expression of Egr2 target genes (Zheng et al., 2013). CD8$^+$ TILs from day 14 tumor-bearing mice were sorted based on high or low expression of Egr2^{EGFP} and analyzed directly for expression of Egr2 targets by qRT-PCR. Two tumors on opposite flanks pooled per mouse. *n* = 3; two independent experiments. (C) Representative flow plots and summary of the 4-1BB/LAG-3 subpopulations in CD8$^+$ Egr2GFP^{hi} and Egr2GFP^{lo} TILs on day 7 and 14. *n* = 4–5. Two independent experiments per time point. (D) Expression of Egr2 targets in the 4-1BB$^+$LAG-3$^+$ and 4-1BB$^-$LAG-3$^-$ subpopulations. The subpopulations were sorted and analyzed directly for the expression of targets by qRT-PCR. Two tumors on opposite flanks were pooled per mouse. *n* = 4; two independent experiments. (E) Egr2$^{flox/flox}$ x pLCKCreERT2 x YFP-Rosa26 mice given five doses of tamoxifen by gavage and inoculated 3 d later with 2 × 10^6 B16.SIY cells. YFP$^+$ or YFP$^-$ CD8$^+$ TILs were sorted and analyzed for *Egr2* transcript directly and after in vitro stimulation. Two tumors on opposite flanks were pooled per mouse. *n* = 3; two independent experiments. (F) Representative flow plots and summary of 4-1BB/LAG-3 coexpression in YFP$^+$ or YFP$^-$ CD8$^+$ TILs on day 7 and 14. *n* = 3; two independent experiments. (G) Expression of *Egr3* and *Hif1*α in

CD8$^+$4-1BB$^+$LAG-3$^+$ TILs are oligoclonal and enriched for tumor antigen specificity

Not all T cells in the tumor microenvironment are specific for tumor-associated antigens, as memory T cells specific for irrelevant antigens are often found among TIL, and nonspecific T cell trafficking has been documented in vivo (Harlin et al., 2006). We hypothesized that the 4-1BB$^+$LAG-3$^+$ CD8$^+$ TILs are tumor-antigen specific because LAG-3, 4-1BB, and Egr2 are up-regulated after TCR stimulation, and our initial characterization suggested that this population expands within the tumor microenvironment in situ. To test this hypothesis, three complementary techniques were used. First, we isolated the CD8$^+$ TILs based on LAG-3 and 4-1BB expression by cell sorting and performed TCRβ spectratype analysis. Compared with the 4-1BB$^-$LAG-3$^-$ TILs and CD8$^+$ splenocytes, the 4-1BB$^+$LAG-3$^+$ TILs had a non-Gaussian distribution and shared one or two dominant peaks (Fig. 3 A). Analysis of several Vβs displaying one dominant peak revealed that Vβ7 contained a single CDR3β sequence shared between the 4-1BB$^-$LAG-3$^+$ and 4-1BB$^+$LAG-3$^+$ populations, indicating a clonal relationship (Fig. 3 A). To measure the oligoclonality of the CDR3β repertoires the Hamming distance (HD) was calculated for each Vβ between the CD8$^+$ TIL subpopulations and the splenic CD8$^+$ population within three separate mice (Fig. S1). By transforming each spectratype into area under the curve frequency profiles, the HD computes the changes in frequency and reports a value of comparison between 0 and 1, with 0 indicating a completely identical frequency profile and 1 signifying a completely discordant profile. As a control, we calculated the HD of the splenic CD8$^+$ populations between different mice (Fig. 3 B, black bar). Because the splenic CD8$^+$ spectratypes are largely Gaussian this value represents the HD between two similar distributions. Analysis of the HD between the CD8$^+$ TIL subpopulations revealed that the 4-1BB$^+$LAG-3$^+$ and 4-1BB$^-$LAG-3$^+$ but not the 4-1BB$^-$LAG-3$^-$ CDR3β distributions are significantly different (less Gaussian) compared with the splenic CD8$^+$ population (Fig. 3 B). These data indicate that the 4-1BB$^+$LAG-3$^+$ and 4-1BB$^-$LAG-3$^+$ populations are oligoclonal expanded subsets of TILs, suggesting likely antigen specificity in these subpopulations.

As a second approach, we used the B16.SIY melanoma and MC38.SIY adenocarcinoma models and monitored CD8$^+$ T cells specific for the H-2K^b–restricted SIY epitope (SIYRYYGL). SIYRYYGL/K^b pentamer$^+$ (H-2K^b/SIY) cells were found in expanded numbers within B16.SIY and MC38.SIY tumors at day 14 after tumor inoculation (Fig. 3 C). Nearly 47% of the H-2K^b/SIY$^+$ cells expressed both 4-1BB and LAG-3, in contrast to 32% of the H-2K^b/SIY$^-$ population (Fig. 3, C and E). This enrichment of antigen-specific CD8$^+$ TILs in the 4-1BB$^+$LAG-3$^+$ populations suggests that these markers identify tumor antigen–specific TILs. The H-2K^b/SIY$^-$ cells also contained significant numbers of 4-1BB$^+$LAG-3$^+$ cells, which is consistent with the notion that tumor antigens other than SIY are also recognized by subsets of CD8$^+$ TILs in vivo (Fig. 3 C). H-2K^b/SIY$^+$ cells in the spleen (unpublished data) or TdLN did not coexpress 4-1BB and LAG-3, indicating that this phenotype is acquired within the tumor microenvironment.

We also analyzed these features in the context of tumor-antigen specific CD8$^+$ TILs in two spontaneously rejected tumor models. To this end, we evaluated H-2K^b/SIY-specific CD8$^+$ TILs cells from MC57.SIY and 1969.SIY tumors. At day 14 after tumor inoculation, ∼5% of the H-2K^b/SIY-specific CD8$^+$ TILs were found in the 4-1BB$^+$LAG-3$^+$ fraction. As with the B16.SIY tumors, no H-2K^b/SIY–specific CD8 T cells coexpressed 4-1BB and LAG-3 in the TdLN or spleen (not depicted; Fig. 3 D). Unlike the B16.SIY and MC38.SIY tumors, no significant enrichment of 4-1BB$^+$LAG-3$^+$ H-2K^b/SIY-specific CD8$^+$ TILs was observed (Fig. 3, D and E). These data suggest that tumor antigen specificity alone does not determine dysfunctionality, and that this is a feature unique to the microenvironment of progressing tumors.

As a third measure to determine if tumor antigen–specific CD8$^+$ T cells acquire the 4-1BB$^+$LAG-3$^+$ phenotype, we transferred congenically marked 2C and P14 Tg T cells, isolated from 2C/Rag2$^{-/-}$ and P14/Rag2$^{-/-}$ mice, into tumor-bearing hosts. The 2C TCR is specific for the SIY model antigen expressed by B16.SIY tumor cells, whereas P14 is an irrelevant TCR specific for the LCMV-derived gp$_{33-41}$ epitope; both TCRs are H-2K^b–restricted. 2C and P14 Tg CD8$^+$ T cells were transferred via tail vein 7 d after tumor inoculation. 7 d after transfer, tumors and TdLNs were extracted and the phenotypic profile of the transferred populations was analyzed. This system allowed for the analysis of two T cell populations with defined antigen specificities within the same tumor microenvironment, as well as the polyclonal host CD8$^+$ T cells. The 2C T cells were more efficiently recruited and expanded within the tumor microenvironment compared with the P14 T cells and encompassed a large fraction of the total CD8$^+$ TIL population (Fig. 3 F). Of the 2C T cells, nearly all expressed LAG-3 and or 4-1BB, whereas this was true for only a small percentage of the P14 cells (Fig. 3, G and H). Consistent with the SIY-K^b pentamer analysis, the coexpression of LAG-3 and 4-1BB on 2C T cells was not observed in the TdLN. Together, these results firmly demonstrate that the 4-1BB$^+$LAG-3$^+$ phenotype is a property of tumor antigen–specific TIL under conditions of tumor progression.

Egr2GFP^{hi} and Egr2GFP^{lo} from day 7 CD8$^+$ TILs isolated from Egr2GFP mice. $n = 5$; two independent experiments. Error bars indicate mean± SEM. *, $P < 0.05$; **, $P < 0.01$; ***, $P < 0.001$. A two-way ANOVA with Bonferroni post-*hoc* test was used for longitudinal studies (A and C) and a Mann-Whitney test was used to compute significance in (B, D–F, and G).

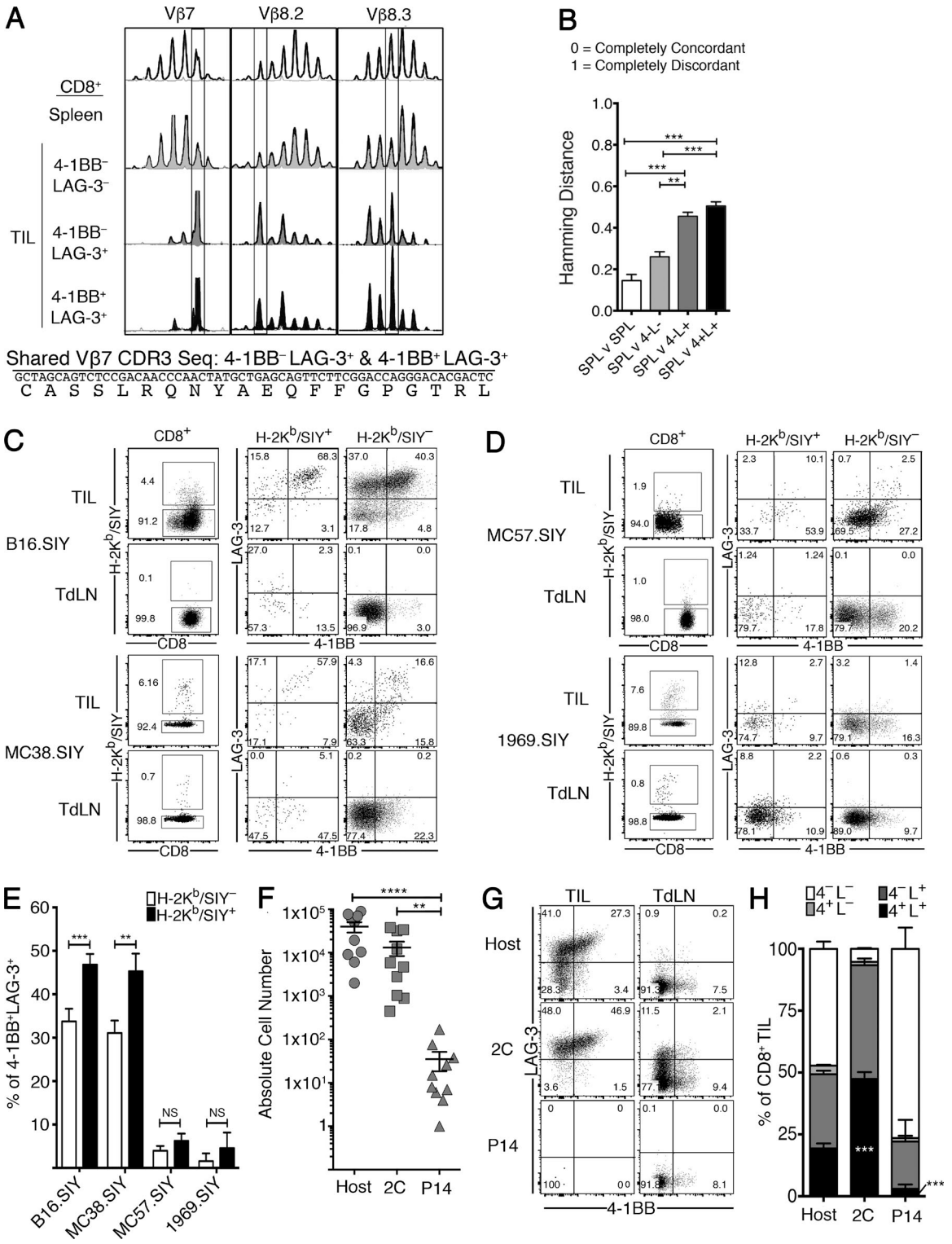

Figure 3. **Co-expression of 4-1BB and LAG-3 identifies tumor antigen–specific TILs in progressing tumors.** (A) Representative CDR3β distributions from the different 4-1BB/LAG-3 subpopulations and CD8⁺ T cells isolated from the spleen. Boxed regions represent dominant peaks in the 4-1BB⁺LAG-3⁺ CD8⁺ TIL subpopulation. (B) As a measure of skewness, the HD for each Vβ spectratype was calculated between each TIL subpopulation and CD8⁺ T cell spleen population within the same mouse. As a control, the HDs from CD8⁺ splenocyte populations between mice (gray bar) were calculated. $n = 3$; one independent experiment. (C and D) Representative flow analysis of the 4-1BB/LAG-3 subpopulation in H-2K^b/SIY⁺ and H-2K^b/SIY⁻ CD8⁺ TILs on day 14 after (C) B16.SIY and MC38.SIY or (D) MC57.SIY and 1969.SIY tumor inoculation. $n = 3$–4; three to five independent experiments. (E) Summary of the composition

CD8$^+$ TILs expressing LAG-3 and 4-1BB exhibit defective IL-2 production yet produce IFN-γ and T reg cell–recruiting chemokines

Based on the characteristics of the in vitro T cell anergy model that led to the identification of Egr2 as an important regulator, we hypothesized that the tumor antigen–specific 4-1BB$^+$LAG-3$^+$ CD8$^+$ TIL population might be dysfunctional in their capacity to produce IL-2. To this end, we sorted each subpopulation and stimulated with anti-CD3 and anti-CD28 mAb, and analyzed IL-2 production by qRT-PCR and ELISA. Because nearly all CD8$^+$ TILs displayed an activated phenotype, we used CD8$^+$CD44$^+$ splenocytes as a positive control. Indeed, the 4-1BB$^+$LAG-3$^+$ cells showed a 100-fold reduction in *Il-2* mRNA, and as much as a 40-fold reduction in IL-2 protein levels, compared with the 4-1BB$^-$LAG-3$^-$ population (Fig. 4, A and B). As a second approach, we examined Egr2^{hi} TIL (which are also largely 4-1BB$^+$LAG-3$^+$) by using the Egr2-GFP reporter mice. Indeed, ex vivo–stimulated Egr2-GFP^{hi} CD8$^+$ TILs also exhibited reduced *Il-2* transcript compared with Egr2-GFP^{lo} cells (Fig. 4 C). As a final approach, we adoptively transferred congenically marked 2C T cells intravenously into tumor-bearing hosts and recovered the 2C T cells 7 d later from the tumor and TdLN. 2C T cells isolated from tumors exhibited a reduced capacity to produce *Il-2* transcripts, at a level equivalent to 4-1BB$^+$LAG-3$^+$ TILs, compared with 2C CD44$^+$ T cells isolated from the TdLN (Fig. 4 D). In chronic infection models, expression of PD-1 has been suggested to identify intrinsically dysfunctional or "exhausted" CD8$^+$ T cells. To determine if PD-1 alone might be sufficient to identify cells that lack the capacity to produce IL-2, we isolated CD8$^+$ TILs that lacked expression of LAG-3 and 4-1BB, and then tested for the ability of the PD-1$^+$ fraction to produce IL-2. Approximately 10% of CD8$^+$ TILs were 4-1BB$^-$LAG-3$^-$PD-1$^+$ on day 14 and 21 (Fig. 4, E and F). Upon ex vivo stimulation, this population retained the capacity to produce *Il-2* mRNA at a level comparable to the 4-1BB$^-$LAG-3$^-$ cells (Fig. 4 G). These results indicate that PD-1 expression alone is not sufficient to identify dysfunctional TIL in the tumor microenvironment.

To further examine functional alterations during tumor progression we tested for protein levels of IL-2, IFN-γ, and TNF after TCR stimulation. As the loss of the ability of CD8$^+$ TILs to produce cytokines is suggested to be a temporal process initiated after entry into the tumor microenvironment (Schietinger et al., 2016; Waugh et al., 2016), or progressively after 30 d in the chronic LCMV model (Wherry et al., 2007), we tested for cytokine production on day 7, 14, 21, and 28. The 4-1BB$^+$LAG-3$^+$ population lost the capacity to produce IL-2 as early as day 7, whereas the 4-1BB$^-$LAG-3$^+$ population lost IL-2 production between day 7 and 14 (Fig. 5 A). Interestingly, the 4-1BB$^-$LAG-3$^-$ population did not lose the ability to produce IL-2 at any time point tested (Fig. 5 A), supporting the notion that this population is not tumor antigen–specific and that differentiation into the dysfunctional state is an antigen-dependent process (Schietinger et al., 2016). Unexpectedly, the 4-1BB$^+$LAG-3$^+$ population produced more IFN-γ at all time points after day 7 compared with their negative counterparts, albeit with a slight decrease in IFN-γ production over time. Although the increase in IFN-γ was maintained until later time points, TNF production was lost by day 28 (Fig. 5 A).

We next evaluated production of cytokines directly in the tumor without in vitro restimulation, which may more closely reflect which T cells were receiving TCR stimulation in situ. Each T cell population was sorted directly ex vivo without any culturing and mRNA levels were measured by qRT-PCR. Elevated *Ifn-γ* and *Gzmb* transcripts were observed from the 4-1BB$^+$LAG-3$^+$ subpopulation, along with a slight decrease in *Tnf-α* levels, compared with the 4-1BB$^-$LAG-3$^-$ cells (Fig. 5 B). As an additional approach, we confirmed production of IFN-γ in primary TILs by injecting tumors with Brefeldin A before analysis by intracellular cytokine staining. Consistent with the mRNA expression, the 4-1BB$^+$LAG-3$^+$ population produced significantly greater amounts of IFN-γ protein (Fig. 5 C). Thus, the 4-1BB$^+$LAG-3$^+$ TIL are not completely devoid of functionality, as they continue to produce IFN-γ despite defective production of IL-2. In fact, this phenotype is consistent with what had been reported previously with in vitro T cell anergy models (Jenkins et al., 1987).

The high level of IFN-γ and *Gzmb* produced by the 4-1BB$^+$LAG-3$^+$ population lead us to hypothesize that this population may still retain cytotoxic capacity. To test this, we performed redirected lysis by co-culturing anti-CD3 bound P815 mastocytoma target cells with the different CD8$^+$ TIL subpopulations directly after sorting. 4-1BB$^+$LAG-3$^+$ CD8$^+$ TILs isolated from day 14 tumors were able to lyse target cells at a comparable efficacy to in vitro primed OT-I cells. 4-1BB$^+$LAG-3$^+$ TILs isolated from day 21 tumors were still able to lyse target cells, albeit to a lesser extent compared with primed OT-I cells (Fig. 5 D).

We have previously shown that CD8$^+$ T cells in the tumor can be the source of the chemokine CCL22 that recruits FoxP3$^+$ regulatory T (T reg) cells to the tumor

of H-2K^b/SIY$^+$ and H-2K^b/SIY$^-$ CD8$^+$ TILs coexpressing 4-1BB and LAG-3 comparing B16.SIY, MC38.SIY, MC57.SIY and 1969.SIY tumors on day 14 after tumor inoculation. $n = 5$; three to four independent experiments. (F and H) On day 7 after tumor inoculation 10^6 P14/CD45.2 and 2C/CD45.1/2 Tg T cells were adoptively transferred, via tail vein, into CD45.1 congenic tumor bearing hosts and analyzed for the (F) total number of recovered cells in the tumor, (G and H) profile of 4-1BB and LAG-3 expression in 2C, P14, and host CD8$^+$ TILs. $n = 5$; two independent experiments. All error bars indicate mean ± SEM. *, $P < 0.05$; **, $P < 0.01$; ***, $P < 0.001$. A Kruskal-Wallis (nonparameteric) test was used for (B) spectratype analysis and (E and F) H-2K^b/SIY analysis. A two-way ANOVA with Bonferroni post-hoc test was used for (H) 2C, Host, and P14 composition analysis.

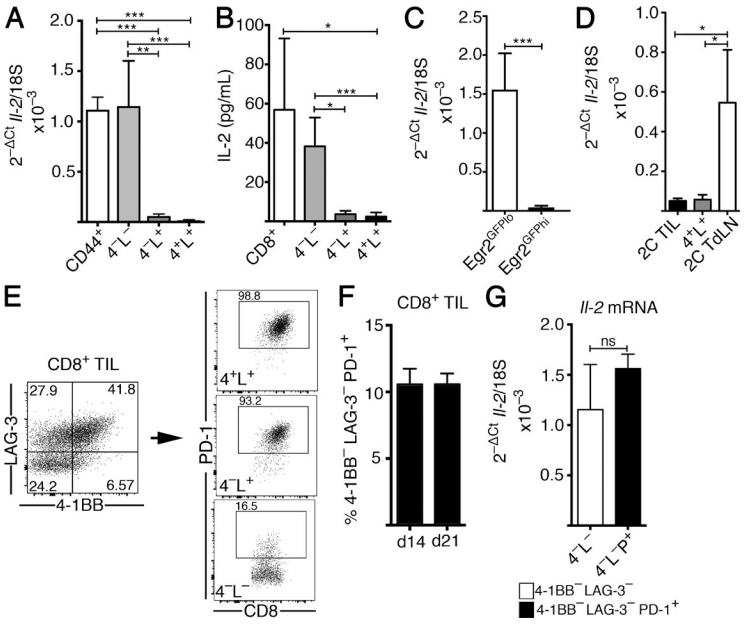

Figure 4. **Co-expression of 4-1BB and LAG-3, but not PD-1, define dysfunctional CD8⁺ TILs with diminished IL-2.** (A and B) Sorted cells from day 14 B16.SIY tumor bearing mice were stimulated in vitro with anti-CD3ε and anti-CD28 for 12 h and analyzed for *Il-2* transcript by qRT-PCR (A) and IL-2 protein by ELISA (B). Two tumors on opposite flanks pooled per mouse. n = 4–5; three independent experiments. (C) Egr2GFP^{hi} and Egr2GFP^{lo} TILs were sorted from day 14 B16.SIY tumor bearing Egr2^{GFP} mice and stimulated in vitro for 12 h and analyzed *for Il-2* transcript by qRT-PCR. Two tumors on opposite flanks pooled per mouse. n = 5; two independent experiments. (D) On day 7 after tumor inoculation 10^6 2C/CD45.1/2 Tg T cells were transferred into mice, and 7 d later, host 4-1BB⁺LAG-3⁺ T cells sorted from the tumor and 2C T cells sorted from the tumor or TdLN were stimulated in vitro and analyzed for expression of *Il-2* transcript by qRT-PCR. Two tumors on opposite flanks pooled per mouse. n = 3; two independent experiments. (E) Representative flow analysis of PD-1 expression on 4-1BB/LAG-3 CD8⁺ TIL subpopulations and (F) summary of the composition of the 4-1BB⁻LAG-3⁻PD-1⁺ subpopulation in the CD8⁺ TIL compartment on day 14 and 21. n = 5; three independent experiments. (G) 4-1BB⁻LAG-3⁻PD-1⁺ and LAG-3⁺4-1BB⁺ CD8⁺ TILs were sorted from day 14 tumor-bearing mice, stimulated in vitro, and analyzed for *Il-2* transcript by qRT-PCR. Two tumors on opposite flanks pooled per mouse. n = 3; two independent experiments. All error bars indicate mean ± SEM. *, $P < 0.05$; **, $P < 0.01$; ***, $P < 0.001$. A Kruskal-Wallis (nonparametric) test was used for analysis of multiple comparisons (A, B, and D) and a Mann-Whitney test was used for pairwise comparisons (C and G).

microenvironment (Spranger et al., 2013). In addition, the chemokine *Ccl1* was an Egr2 target in anergic T cells (Zheng et al., 2013), and previous work had suggested that CCL1 also could contribute to T reg cell recruitment in the tumor context in vivo (Hoelzinger et al., 2010). However, whether all CD8⁺ T cells in the tumor produce these chemokines or if they are only produced by subpopulations of T cells had not been determined. To address this, we analyzed the CD8⁺ TIL phenotypic subpopulations for *Ccl1* and *Ccl22* mRNA expression directly ex vivo by qRT-PCR. Indeed, the 4-1BB⁺LAG-3⁺ TIL population produced substantially greater *Ccl1* and *Ccl22* compared with their negative counterparts or to splenic CD8⁺CD44⁺ T cells (Fig. 5 E). As a control, expression of a distinct chemokine *Ccl5* was found not to be differentially expressed (unpublished data). Together, these data show that coexpression of 4-1BB and LAG-3 delineates tumor antigen–specific CD8⁺ TIL that lack the ability to produce IL-2 yet retain the ability to produce IFN-γ, kill target cells in vitro, and secrete chemokines capable of T reg cell recruitment. Given the fact that IFN-γ is responsible for the up-regulation of PD-L1 and IDO in the tumor microenvironment, and that chemokines produced by CD8⁺ TIL contribute to T reg cell recruitment (Spranger et al., 2013), these data suggest the possibility that the 4-1BB⁺LAG-3⁺ population might contribute to the network of immune-suppressive mechanisms within the tumor microenvironment that limit the efficacy of antitumor immunity.

Gene expression profiling reveals that CD8⁺4-1BB⁺LAG-3⁺ TILs express an extensive array of additional co-stimulatory and co-inhibitory receptors

Having in hand surface markers that appeared to define tumor antigen–specific dysfunctional CD8⁺ TILs, we wanted to compare the gene expression profile of this population to other published profiles of dysfunctional CD8⁺ T cells to determine genes that may regulate or be used to profile cells in this dysfunctional state. To this end, we conducted a cross-study comparison of the transcriptional profiles of the dysfunctional 4-1BB⁺LAG-3⁺ CD8⁺ TILs, hypofunctional CD8⁺ TILs from a study using the murine CT26 tumor model (Waugh et al., 2016), and LCMV-exhausted, GP33-specific CD8⁺ T cells (Doering et al., 2012). We only considered genes with a twofold increase over controls from each study independently. Over a twofold greater number of genes was found to be shared between our current the dysfunctional TIL dataset and the previously published hypofunctional CD8⁺ TIL data, than with the exhausted T cell profile (Fig. 6 A and Table S2). In addition, a rank-rank hypergeometric overlap (RRHO) analysis indicated a greater statistically significant overlap (Fig. S3 A) and a greater correlation (Fig. S3 B) between the current dysfunctional TIL and the published hypofunctional CD8⁺ TIL gene expression profiles compared with the virally induced exhausted CD8⁺ T cell profile, suggesting a more similar molecular program between CD8⁺ T cells isolated from tumors compared with chronic viral infection.

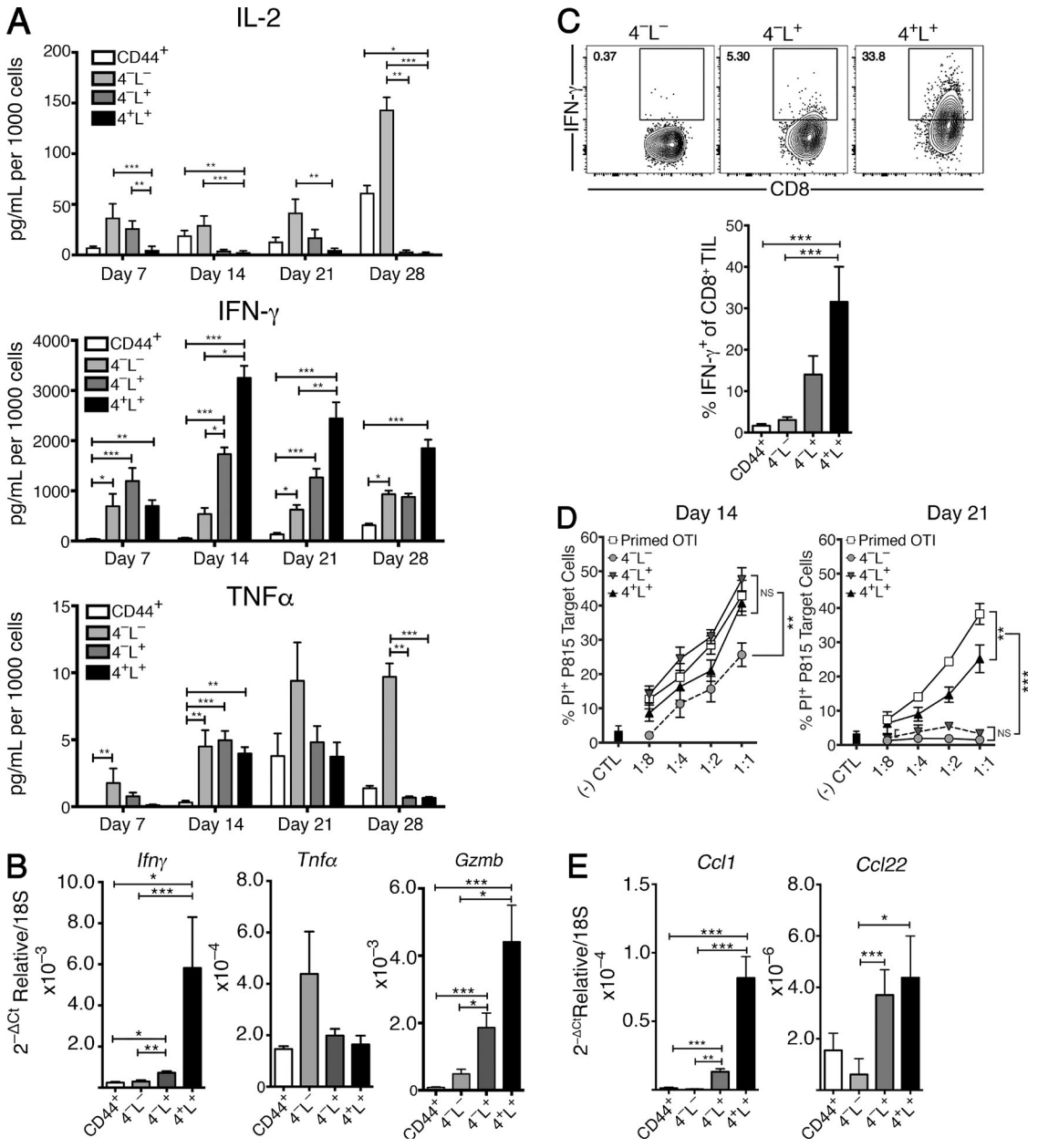

Figure 5. **Dysfunctional CD8⁺ TILs retain IFN-γ production, cytolytic capacity, and produce T reg cell–recruiting chemokines.** (A) Longitudinal analysis CD8⁺ TIL subpopulation cytokine production capacity. CD8⁺ TIL subpopulations were sorted and stimulated with anti-CD3ε and anti-CD28 for 10–12 h and the concentration of IL-2, IFN-γ, and TNF was measured. Concentration was normalized to cell number. Two tumors on opposite flanks pooled for day 7 and 14. $n = 4–5$; two independent experiments. (B) *Ifn-γ*, *Tnf-α*, and *Gzmb* transcript levels in the 4-1BB/LAG-3 subpopulations analyzed directly ex vivo. Two tumors on opposite flanks pooled per mouse. $n = 3–5$; three independent experiments. (C) Representative flow plot and summary of IFN-γ production analyzed directly ex vivo. In brief, 100 µl of PBS containing 2 mg/ml GolgiPlug was injected intratumorally on day 14 after tumor inoculation. 8 h later, TILs were isolated. All steps were performed on ice with media containing 1 mg/ml GolgiStop until fixation. $n = 5$; two independent experiments. (D) CD8⁺ TIL subpopulations at indicated time points were sorted and plated with 50,000 P815 target cells and 1 µg/ml anti-CD3ε. Lysed target cells were measured by positive staining for propidium iodine and/or live/dead fixable viability dye. P815 target cells plated without CTLs were used as a negative control (black bar). Primed OTI cells were used as a positive control. Tumors from 10 mice with two tumors on opposite flank were pooled to obtain sufficient quantities of CD8⁺ TILs. Data are representative of three independent experiments. (E) *Ccl1* and *Ccl22* transcript levels in the 4-1BB/LAG-3 subpopulations analyzed directly ex vivo by qRT-PCR. $n = 4$; two independent experiments. All error bars indicate mean ± SEM. *, $P < 0.05$; **, $P < 0.01$; ***, $P < 0.001$; ****, $P < 0.0001$. A Kruskal-Wallis (nonparametric) test was used for (A–C and E) cytokine/chemokine analysis and a two-way ANOVA with Bonferroni post-hoc test was used for cytolytic assay (D).

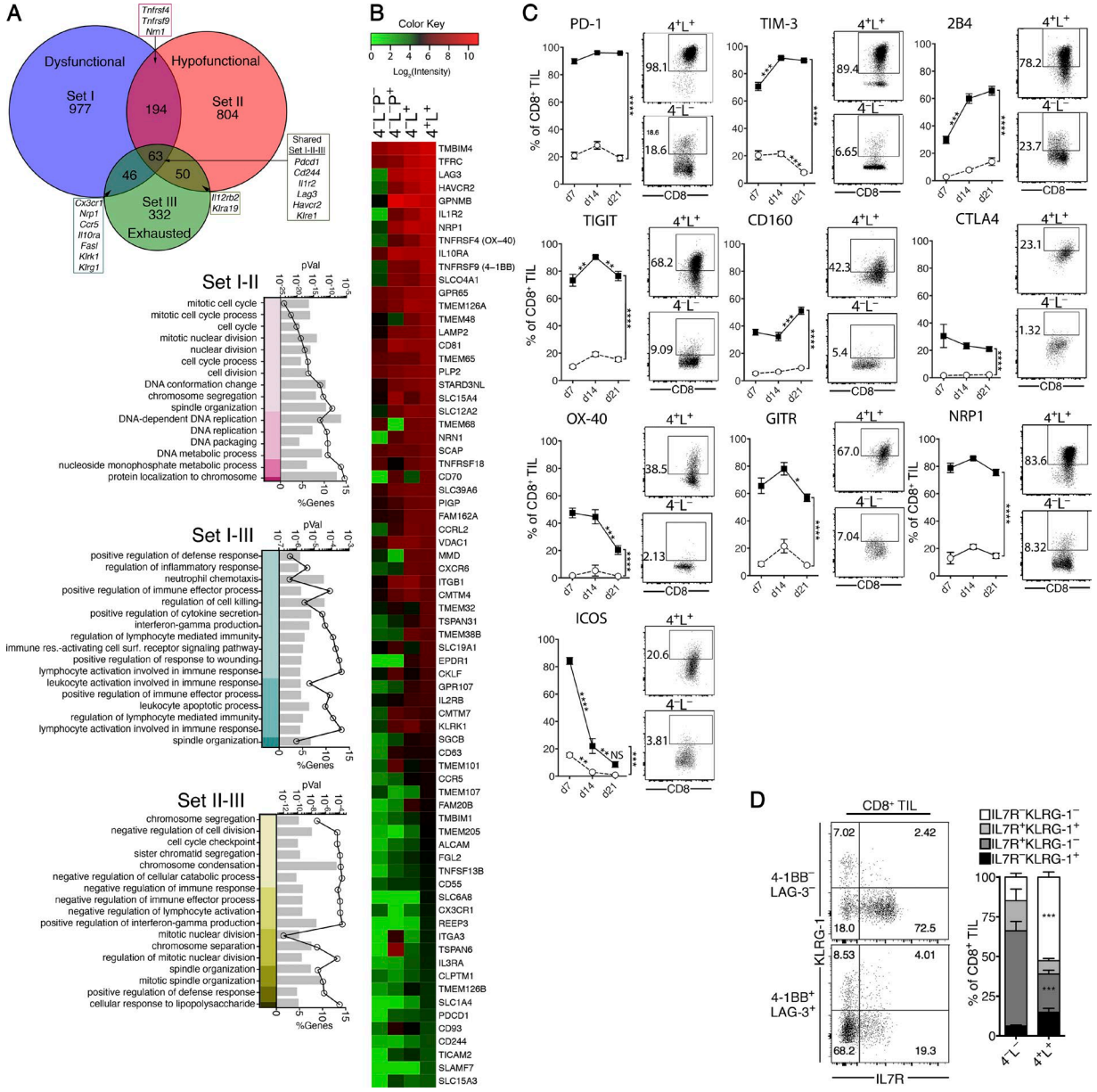

Figure 6. **Dysfunctional CD8⁺ TILs express a wide range of co-inhibitory and co-stimulatory receptors.** (A and B) Gene expression profile of cell surface receptors in the 4-1BB/LAG-3 CD8⁺ TIL subsets. Probe sets that revealed a 1.5-fold increase in the 4-1BB⁺LAG-3⁺ population relative to the 4-1BB⁻LAG-3⁻PD-1⁻ population are displayed. Columns show the $\log_2$-transformed signal intensity. (C) Longitudinal study of selected up-regulated cell surface receptors. Flow plots are representative of the CD8⁺ TIL subsets on day 14. $n = 5$; two to five independent experiments for each time point. (D) Representative flow plot and summary of KLRG-1 and IL-7Rα expression among the 4-1BB/LAG-3 subpopulations on day 14 after tumor inoculation. $n = 5$; two independent experiments. All error bars indicate mean ± SEM. *, $P < 0.05$; **, $P < 0.01$; ***, $P < 0.001$; ****, $P < 0.0001$. A two-way ANOVA with Bonferroni post-hoc test was used for all analyses.

To investigate the molecular pathways between these three populations, we grouped gene ontology networks into nodes and determined the most significant pathways within each node (Fig. 6 A; and Tables S3 and S4). Interestingly, gene ontology (GO) terms shared between our dysfunctional T cell dataset and the published hypofunctional T cell dataset were greatly enriched in cell cycle genes, consistent with our observation that the dysfunctional population is largely Ki67⁺. GO terms shared between dysfunctional and exhausted gene sets encompassed effector programs, such as regulation of cell killing, chemotaxis, and interferon-γ production. GO terms shared between hypofunctional and exhausted gene sets consisted of cell cycle pathways, negative regulation of lymphocytes, and interferon-γ production. These data suggest that

although some conserved molecular programs likely exist in these dysfunctional differentiation states, many pathways may be differentially regulated between chronic viral infections and in the tumor context.

Whereas many inhibitory receptors, including *Pdcd1* (PD-1), *Havcr2* (TIM-3), *Cd244* (2B4), *Klre1*, and *Lag3* were shared between all datasets; the co-stimulatory receptors *Tnfrsf4* (OX-40) and *Tnfrsf9* (4-1BB) were up-regulated in dysfunctional and hypofunctional $CD8^+$ TIL datasets. Therefore, to enrich in potential markers and therapeutic targets on tumor-specific $CD8^+$ TILs, we aimed to characterize the complete cell surface phenotype of the 4-1BB$^+$LAG-3$^+$ CD8 TIL population. Comparing the different $CD8^+$ TIL subpopulations, we found several additional up-regulated co-stimulatory receptors: *Tnfrsf18* (GITR), *Nkg2d* (KLRK1), and *Cd27*. The transcript for *Nrp1* (neuropilin-1), which encodes for a cell surface receptor protein implicated in $CD4^+$ T reg cell function (Sarris et al., 2008), was also highly expressed. We confirmed expression of many of these molecules by flow cytometry at day 7, 14 and 21 after tumor inoculation (Fig. 6 C). We also extended our analysis to include the co-stimulatory molecule ICOS and the inhibitory receptors CD160 and TIGIT because ICOS and CD160 were close to the cutoff value, and no probe was present for TIGIT in the gene array. In addition, recent studies indicate that targeting these receptors can be therapeutic in murine models of cancer (Fan et al., 2014; Johnston et al., 2014). PD-1, TIG IT, TIM-3, CD27, and NRP1 were expressed the majority of the 4-1BB$^+$LAG-3$^+$ TIL population and expression was maintained over time. 2B4, CD160, CTLA4, OX-40, and GITR subdivided a lesser fraction of the 4-1BB$^+$LAG-3$^+$ population. The expression of several inhibitory receptors, 2B4, TIM3, and CD160 increased over this 3-wk time frame, whereas expression of the co-stimulatory receptors, ICOS, and OX-40, decreased (Fig. 6 C).

To address if the dysfunctional $CD8^+$ TILs are terminally differentiated short-term effector cells or memory-like cells, we additionally analyzed the expression of KLRG-1 and IL-7Rα (Joshi et al., 2007). Most of the $CD8^+$ TIL were negative for KLRG-1 expression and there was no difference between the 4-1BB$^+$LAG-3$^+$ and 4-1BB$^-$LAG-3$^-$ populations. However, the majority of the 4-1BB$^+$LAG-3$^+$ TIL did not express the IL-7 receptor (IL-7Rα) compared with their negative counter parts (Fig. 6 D). These results suggest that the 4-1BB$^-$LAG-3$^-$ TIL, which are not apparently specific for antigens expressed in the tumor microenvironment, are more memory-like, yet at the same time, the tumor antigen–specific LAG-3$^+$4-1BB$^+$ subset has not fully acquired a terminal effector phenotype.

Targeting 4-1BB and LAG-3 exerts antitumor activity in vivo and normalizes the function and phenotypic composition of $CD8^+$ TILs

Although it was conceivable that LAG-3 and 4-1BB were just phenotypic markers for dysfunctional tumor antigen–specific $CD8^+$ TIL, it was of interest to assess whether targeting these receptors might have therapeutic utility. To this end, an agonistic anti–4-1BB mAb was administered alone or in combination with a blocking anti–LAG-3 mAb in mice bearing established B16.SIY tumors. Although each antibody treatment alone had some therapeutic effect as reflected by slower tumor growth, the combination was particularly potent (Fig. 7 A). Analysis of the tumor microenvironment revealed that improved tumor control with the combination therapy was accompanied by an increase in the number of $CD8^+$ TILs specific for the SIY antigen (Fig. 7 B), consistent with results reported previously with anti–PD-L1 + anti–CTLA-4 mAb (Spranger et al., 2014; Twyman-Saint Victor et al., 2015).

We next examined whether the therapeutic effect of anti–4–1BB + anti–LAG-3 mAbs was associated with a loss of phenotypic markers defining dysfunctional T cells in the steady state. We were concerned that reanalyzing the T cells for expression of LAG-3 and 4-1BB might be problematic, as the administered Abs could theoretically modulate the target receptors from the cell surface. To this end, we took advantage of the coordinate expression of additional receptors as identifiedin Fig. 6 by gene expression profiling. Preliminary analyses of the bulk TIL subpopulations revealed decreased expression of NRP1 and 2B4 after anti–LAG-3 + anti–4-1BB treatment (unpublished data). We therefore analyzed coexpression of 2B4 and NRP1 on SIY-reactive $CD8^+$ TILs identified by pentamer staining. Indeed, a 2.7-fold decrease in the coexpression of 2B4 and NRP1 was observed upon anti–4-1BB + and anti–LAG-3 mAb treatment (Fig. 7 C), indicating a loss of the surface phenotype associated with T cell dysfunction. To determine whether this change was accompanied by a shift toward an effector phenotype, expression of KLGR-1 was examined. Indeed, a marked increase in KLGR-1 expression was observed on the SIY-reactive TIL after treatment, and a 3.7-fold increase in the KLRG-1^{hi}IL-7Rα^{lo} population was observed (Fig. 7 D).

It was conceivable that treatment with anti–LAG-3 + anti–4-1BB mAbs was not altering the phenotype of T cells already within the tumor, but rather was supporting recruitment of newly primed functional T cells from secondary lymphoid organs. To distinguish these possibilities, we used the S1PR inhibitor FTY720, which prevents T cell egress from lymph nodes (Halin et al., 2005). We had previously shown that the efficacy of anti-PD-L1-based immunotherapies was preserved in the presence of FTY720, arguing for refunctionalization of TIL as the major mechanism of action (Spranger et al., 2014). FTY720 administration was started on day 6 after tumor inoculation, 24 h before the start of anti-LAG-3 + anti-4-1BB treatment, and continued every day until TIL analysis on day 14. Peripheral blood analyzed at the same time point revealed marked depletion of circulating T cells (Fig. S2). Despite this loss of circulating T cells, the down-regulation of 2B4 and NRP1 and the shift toward the KLRG1^{hi}IL-7Rα^{lo} phenotype was nonetheless preserved (Fig. 7, E and F).

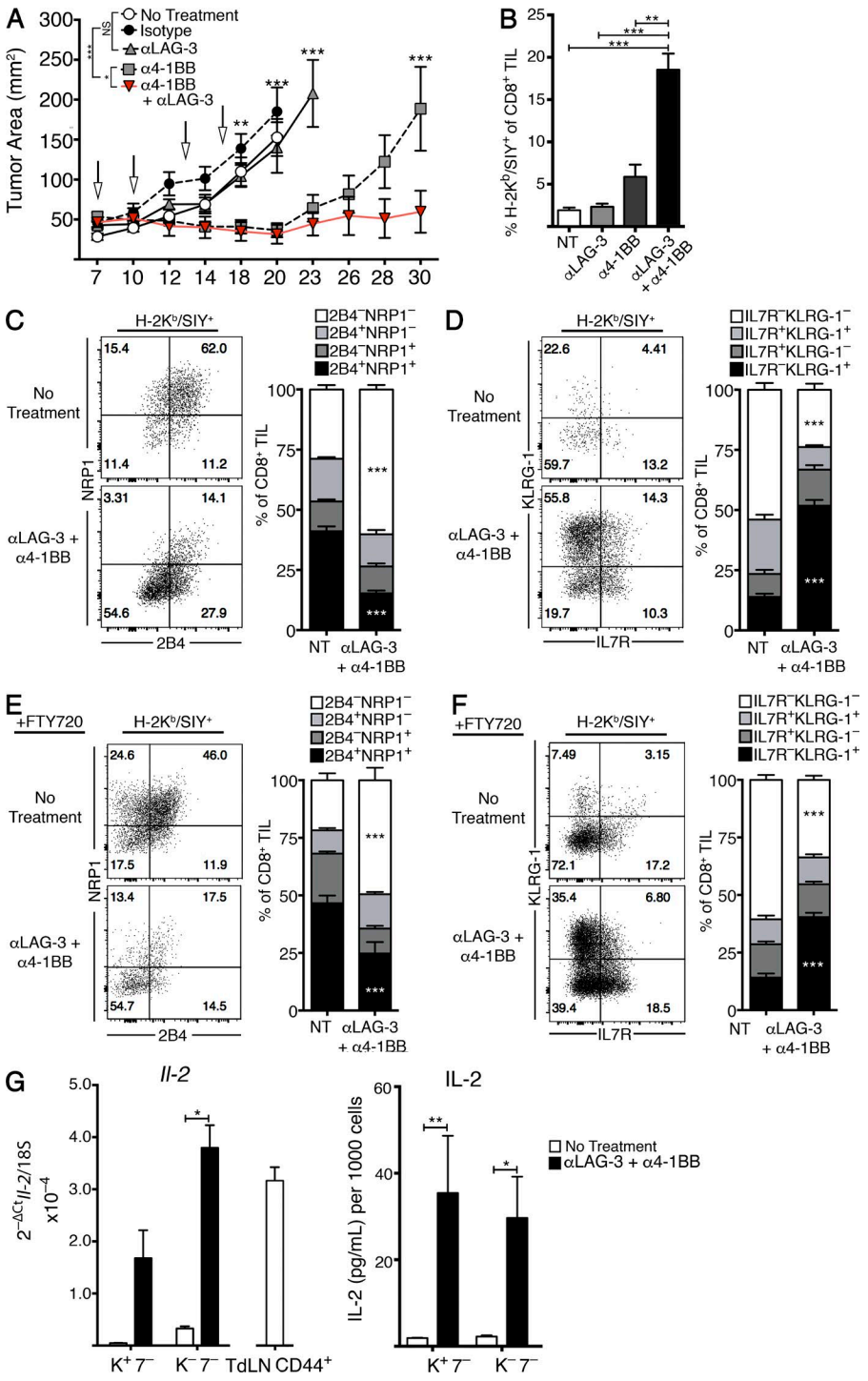

Figure 7. **Anti-4-1BB and anti-LAG-3 acts synergistically to control tumor outgrowth and restore TIL function.** (A) Tumor outgrowth measured in mm^2. Arrows indicate on which days mice received antibody therapy. Statistical significance at indicate time points is in comparison to anti-4-1BB + anti-LAG-3 treatment. *n* = 5; two independent experiments. (B) Composition of H-2K^b/SIY$^+$ CD8$^+$ TILs on day 14. Mice received antibody doses (100 µg each) on days 7, 10, 13, and 16. *n* = 5; two independent experiments. (C–F) Representative flow plot and summary of NRP1/2B4 (C and E) and KLRG-1/IL-7Rα (D and F) expression in H-2K^b/SIY$^+$ CD8$^+$ TILs without FTY720 (C and D) and with FTY720 (E and F) on day 14 after tumor inoculation. Mice received antibody treatment as in (A and B) and FTY720 was administered at a dose of 25 µg/mouse by gavage starting one day before treatment and continuing one dose per day until analysis (day 6 to day 13). *n* = 5; two independent experiments. (G) IL-2 production after treatment. Sorted cells from treated or untreated day 14 B16.SIY tumor bearing mice were stimulated in vitro for 12 h and analyzed for *Il-2* transcript by qRT-PCR. Protein concentration was determined by the bead-based LEGENDplex immunoassay and normalized to cell number. Two tumors on opposite flanks pooled per mouse. *n* = 2–3; two independent experiments. A two-way ANOVA with Bonferroni post-*hoc* test was used for all analyses. All error bars indicate mean ± SEM. *, $P < 0.05$; **, $P < 0.01$; ***, $P < 0.001$.

To examine functional restoration of the TIL, we sorted the KLRG-1^{lo}IL-7Rα^{lo} and KLRG-1^{hi}IL-7Rα^{lo} CD8$^+$ TIL populations from B16.SIY tumors on day 14 following treatment and analyzed for IL-2 after restimulation in vitro. Indeed, the KLRG-1^{lo}IL-7Rα^{lo} and KLRG-1^{hi}IL-7Rα^{lo} populations showed an increased capacity to produce IL-2 upon stimulation (Fig. 7 G). The relative level of *Il-2* mRNA was comparable between the two CD8$^+$ TIL populations and control CD8$^+$CD44$^+$ TdLN T cells. Collectively, these data suggest that anti-4-1BB/anti-LAG-3 combinatorial treatment induces significant changes in the phenotype profile and promotes functional restoration of tumor antigen–specific CD8$^+$ T cells already present within the tumor microenvironment.

DISCUSSION

Dysfunction of tumor antigen–specific TIL is characteristic of the T cell–inflamed tumor microenvironment phenotype, and likely explains the paradox of progressing tumors in the face of ongoing immunity. However, identifying tumor antigen–specific TIL among the background of passively trafficking irrelevant T cells, and understanding this phenotype as a differentiation state, had been hampered by a lack of accurate surface markers. Based on our previous work identifying the transcription factor Egr2 as a critical regulator of $CD4^+$ T cell anergy under reductionist conditions in vitro, we applied knowledge of Egr2 targets to evaluate applicability of these markers toward understanding dysfunctional T cells within tumors in vivo. Our current data indeed confirm that coexpression of LAG-3 and 4-1BB is sufficient to identify the majority of tumor antigen–specific $CD8^+$ T cells within the tumor microenvironment. Co-expression of these markers was not observed within peripheral lymphoid organs in tumor-bearing mice, suggesting that a property unique to the tumor context drives 4-1BB and LAG-3 expression. In addition, acquisition of LAG-3 and 4-1BB expression was not observed within tumors that were undergoing successful rejection, arguing that the acquisition of this phenotype occurs under conditions of incomplete antigen clearance.

Although the molecular characterization of anergic $CD4^+$ T cells in vitro provided the foundational information that enabled the study of dysfunctional $CD8^+$ TIL in vivo, it is clear that these two T cell states are not identical and only partially overlapping. Egr2 was expressed in a subpopulation of $CD8^+$ TILs and this population was enriched in several Egr2 target genes, including 4-1BB and LAG-3. However, Egr2 expression did not define the entire population of 4-$1BB^+$LAG-3^+ TIL. In addition, conditional deletion of Egr2 in T cells only showed a partial functional role of Egr2 in regulating 4-1BB and LAG-3 expression, suggesting that other factors such as HIF-1α and Egr3 might compensate in the regulation of these receptors. In addition, NF-κB and NFAT/AP-1 have been implicated in 4-1BB expression after TCR stimulation (Kim et al., 2003; Martinez et al., 2015). It will be of interest to elucidate the full transcription factor network that mediates the dysfunctional state of $CD8^+$ TIL in vivo, as inhibiting these pathways could lead to novel immunotherapeutics.

Significant effort has been aimed at understanding the molecular mechanisms of T cell dysfunction using various model systems, both in vitro and in vivo. The term T cell anergy was originally applied to describe a hyporesponsive state resulting from TCR ligation in the absence of co-stimulation in $CD4^+$ Th1 clones (Schwartz et al., 1989). However, the term T cell anergy has since been used to describe many different types of tolerance phenomena (Schwartz, 2003). T cell exhaustion was originally described in models of chronic viral infection, particularly the LCMV clone 13 model (Zajac et al., 1998). It has been assumed that the similarities between chronic infection and progressing tumors, such as persistent antigen exposure and involvement of negative regulatory pathways, implied an identical or similar dysfunctional state in these two disease contexts (Schietinger and Greenberg, 2014). Indeed, many of the co-inhibitory receptors expressed on $CD8^+$ TILs and exhausted virus-specific T cells are shared, as is a component of the gene expression network (Fig. 6 A; Baitsch et al., 2011; Kuchroo et al., 2014). However, the mechanisms inducing and maintaining $CD8^+$ TIL dysfunction are likely regulated by additional factors that differ between chronic infections and cancer, such as the balance between metabolic provision and demands on the T cells (Pearce et al., 2013), as well as the tissue localization of the effects. In addition, T cells in different tumor microenvironments could differentiate into unique dysfunctional states. Therefore, it may be preferable to describe this phenotype more descriptively, as T cell dysfunction within the tumor microenvironment rather than anergy or exhaustion. Furthermore, our current work emphasizes that the term dysfunction does not imply complete lack of function. Indeed, cytolytic capacity of the 4-$1BB^+$LAG-3^+ population was retained as analyzed directly ex vivo. Therefore, the failure of the endogenous immune response to eliminate the tumor does not appear to be attributable to a lack of intrinsic cytolytic activity by antigen-specific T cells.

The induction of T cell exhaustion during chronic infection is thought to be a mechanism to limit collateral damage to the host (Goldszmid et al., 2014) and type I and type II IFNs have been implicated in both proinflammatory and immune-regulatory roles in chronic infection (Snell and Brooks, 2015; Cunningham et al., 2016). Therefore, it seems plausible that dysfunctional antigen-specific $CD8^+$ TIL may contribute to the overall immune suppressive network within the tumor microenvironment. IFN-γ produced by antigen-specific $CD8^+$ TILs results in up-regulation of PD-L1 on tumors cells and IDO expression by infiltrating myeloid cells (Spranger et al., 2013). In addition, the production of the chemokines CCL22 and CCL1 by these cells likely contributes to T reg recruitment into the tumor microenvironment. We previously had shown that PD-L1 and IDO up-regulation, as well as T reg cell accumulation within the tumor, all depend on $CD8^+$ T cells (Spranger et al., 2013), and our current work has indicated that the 4-$1BB^+$LAG-3^+ subset is the major source of IFN-γ and chemokines mediating these effects. Thus, the dysfunctional $CD8^+$ TIL might be viewed as part of the regulatory network from this perspective. Further work will be needed to understand the full functional contribution of these cells to immune regulation within the tumor microenvironment.

The use of 4-1BB and LAG-3 as markers of dysfunctional tumor-reactive T cells enabled flow cytometric sorting for gene expression profiling without altering transcript levels that could be caused by TCR ligation through MHC/multimer binding. Comparison of two tumor-specific dysfunctional $CD8^+$ TIL gene expression profiles to the LCMV-specific exhausted profile indicated a greater overlap of the

transcriptional signatures in the tumor context. In addition, pathways regulating the cell cycle were enriched among the $CD8^+$ TIL profiles, suggesting that steady-state proliferation may be an additional characteristic of the dysfunctional state within the tumor microenvironment. Gene expression analysis also revealed up-regulated transcripts encoding additional co-inhibitory receptors, but also several co-stimulatory receptors. This latter observation was unexpected based on the phenotype of dysfunctional $CD8^+$ T cells in chronic infection models (Crawford et al., 2014; Kuchroo et al., 2014). Observations in these models suggest that co-stimulatory receptor expression on exhausted $CD8^+$ T cells is expressed at low levels or wanes over time (Wherry et al., 2007; Clouthier et al., 2014; Crawford et al., 2014). On the contrary, dysfunctional $CD8^+$ TIL continually expressed several co-stimulatory receptors (4-1BB, OX-40, and GITR). These data suggests a scenario in which persistently activated $CD8^+$ TILs are in a state of chronic activation and are awaiting engagement by co-stimulatory ligands, which might be inadequately available within the tumor microenvironment. This notion is consistent with the therapeutic effect of combined 4-1BB ligation added to LAG-3 blockade, which might be viewed as rescuing TIL from a paucity of 4-1BB signaling. The net composition of ligands for co-stimulatory versus co-inhibitory receptors within the tumor could contribute to the ultimately functional phenotype of tumor antigen–specific TIL and will be an interesting question to pursue in future studies.

Our gene expression profiling of the dysfunctional $CD8^+$ TIL population allowed us to determine additional cell surface receptors coexpressed by this population and track these markers during antibody therapy. Although the significant decrease in NRP1 and 2B4 and increase in KLRG-1 expression in the tumor-specific H-$2K^b$/SIY^+ suggests a phenotypic response in the 4-$1BB^+$LAG-3^+ TIL subset, it remains possible that a precursor population found in the 4-$1BB^-$LAG-3^- subset could be a source of precursor cells for the observed changes in the $CD8^+$ TIL population overall. We believe this is unlikely, due to several observations. First, ∼17% of H-$2K^b$/SIY^+ $CD8^+$ TILs are found in the 4-$1BB^-$LAG-3^- subpopulation and, because transcript levels of *Tnfrsf9* (4-1BB) and *Lag3* do not change upon treatment (unpublished data), it remains likely that the phenotypic changes occur in the 4-$1BB^+$LAG-3^+ subpopulation. Second, the 4-$1BB^-$LAG-3^- population displays a phenotype closely resembling memory precursor effector cells (MPEC; KLRG-1^{lo}IL-$7R\alpha^{hi}$ $CD44^+$), which are thought to not give rise to short-lived effector cells (SLEC; KLRG-1^{hi}IL-$7R\alpha^{lo}$; Kaech et al., 2003; Sarkar et al., 2008). Although we do not formally prove a direct causal relationship between antibody treatment and phenotypic changes in the 4-$1BB^+$LAG-3^+ population, indirect evidence suggests that this is the case.

Our previous work had suggested that restoration of IL-2 production in the $CD8^+$ TIL compartment strongly correlated with the therapeutic efficacy of anti-CTLA-4 + anti–PD-L1 or combined with an IDO inhibitor (Spranger et al., 2014). Our current results also identified restored IL-2 production by tumor antigen–specific $CD8^+$ TILs in response to anti–4-1BB + anti–LAG-3 therapy. Thus, restoration of IL-2 might be a useful pharmacodynamic biomarker to be measured in posttreatment biopsies in patients participating in immunotherapy clinical trials. However, it is not yet known if restored IL-2 production is functionally important for antitumor T cell efficacy or serves as a correlate to refunctionalized $CD8^+$ TILs, a possibility that should be investigated in future studies.

Both anti–4-1BB and anti–LAG-3 mAbs are being tested in early phase clinical trials, and it is attractive to consider a combination study in human cancer patients. The ability of $CD8^+$ TILs to up-regulate KLRG-1 and down-regulate 2B4 and NRP1 expression could be the result of additional translational biomarkers. As some patients do not respond to anti–PD-1-based therapies, novel combinations may have utility in such individuals. Moreover, the additional co-stimulatory and co-inhibitory receptors identified in our current work could represent functionally relevant targets for new immunotherapy strategies.

MATERIALS AND METHODS

Mice and tumor inoculation

Female C57BL/6 mice ranging from 6 to 8 wk of age were purchased from Taconic Farms. CD45.1 and $Rag2^{-/-}$ mice on the C57BL/6 background were obtained from Taconic Farms and bred at the University of Chicago (Chicago, IL). 2C/$Rag2^{-/-}$ and P14/$Rag2^{-/-}$ mice have been previously described (Brown et al., 2006). $Egr2^{flox/flox}$ mice were a gift from H. Singh (University of Chicago, Chicago, IL), and pLCK-CreERT2 x ROSA-YFP mice were generated in our laboratory and have been previously described (Evaristo et al., 2016). B16.SIY.dsRed (Kline et al., 2012), C1498.SIY.GFP (Zhang et al., 2009), and MC57.SIY.GFP (Spiotto et al., 2002) tumor cells were engineered to express either dsRed or GFP in frame with the H2-K^b–restricted model antigen SIYRYYGL. The 1969.SIY.GFP cell line was engineered by retroviral transduction of the 1969 cell line (Diamond et al., 2011) using the pLEGFP plasmid expressing cDNA for SIY RYYGL (Spiotto et al., 2002). For experiments, mice 6–9 wk of age received 2×10^6 tumor cells s.c. on either the left flank or both the left and right flank. All mice were maintained according to the National Institute of Health Animal Care guidelines and studied under IACUC-approved protocols.

To generate the targeting construct for the $Egr2^{EGFP}$ knock-in reporter mice, a 12.6-kb mouse genomic DNA fragment, including the *egr2* gene, was excisedwith SacII and cloned into a pEasy-Flox vector adjacent to the thymidine kinase selection marker. A cassette containing IRES2-eGFP and a LoxP-flanked neomycin selection marker was inserted into an Nhel site between the translation stop codon and the polyadenylation signal of the *egr2* gene. ES cell clones from 129 mice were electroporated and selected for Neomycin resistance. ES cell clones were verified for homologous in-

sertion in the endogenous locus by PCR and Southern blot with 5′ and 3′ probes. Mice were backcrossed to C57BL/6 for more than eight generations.

TIL isolation

Tumors were harvested from mice at the indicated time points. Tumors were dissociated through a 50-µm filter and washed with PBS. TILs were further enriched by layering Ficoll-Hypaque beneath the cell suspension, followed by centrifugation without breaks for 15–30 min at 400 *g*. The buffy layer was isolated and washed twice with PBS before staining. For isolating specific cell populations by FACS, tumors were pooled when indicated, and the cell layer was repurified by Ficoll-Hypaque centrifugation twice. For day 28 tumors, after Ficoll-Hypaque separation, T cells were further purified by negative bead selection according to manufacturer's instructions (MagniSort; eBioscience). Cells were then washed with PBS and stained at 4°C for 15 min before resuspending in complete DMEM (cDMEM: 10% FBS, 100 U/ml Penicillin-Streptomycin, 1% MEM Non-Essential Amino Acids, 50 µM β-ME, and 0.01 M MOPS), and were sorted into either RLT lysis buffer (QIAGEN) or cDMEM, depending on the experimental assay. Cells sorted into RLT buffer were put directly on dry ice as soon as the sort was finished.

Flow cytometry and antibodies

Cell suspensions were washed twice in PBS before staining an FACS buffer (2% FBS, 2 mM EDTA, and 0.001% NaN_3). Cells were stained for 30 min on ice and fixed in 1% PFA. Antibodies against the following molecules were used: CD3 (17A2, AX700), 2B4 (2B4, FITC), CD127 (A7R34, PE), OX-40 (OX-86, PE), 4-1BB (17B5, Biotin, APC), CD160 (7H1, PE-Cy7), LAG-3 (C9B7W, PerCPeFluor710), PD-1 (RMP1-30, PE-Cy7), NRP1 (3E12, BV421), GITR (DTA-1, FITC), ICOS (7E.17G9, BV421), KLRG-1 (2F1, eF450, BV605), TIGIT (1G9, APC), TIM-3 (RMT3-23, PE), CD4 (RM4-5, BV605), CD45.1 (A20, FITC), CD45.2 (104, PE), and CD8α (53–6.7, BV711). Fixable Viability Dye 506 (eBioscience) was used for live/dead discrimination. Staining of SIY-specific T cells was performed using the SIYRYYGL-Pentamer (PE; Proimmune); a SIINFEKL-pentamer was used as a nonspecific control. All flow cytometric analysis was conducted on an LSRFortessa (BD) and analyzed using FlowJo software (Tree Star).

Quantitative real-time PCR

Total RNA was extracted from sorted cell populations using the RNEasy Micro kit (QIAGEN) following the manufacturer's protocol. cDNA was synthesized using the High Capacity cDNA Reverse Transcription kit (Applied Biosystems) according to manufacturer's instructions. Transcript levels were determined using primer-probe sets (Table S1) developed through the online ProbeFinder Software and the Universal Probe Library (Roche) with the exception of IL-2 (Mm00434256_m1) and 18S (Hs99999901_s1). To minimize batch effect, when possible, all samples probed for a gene were run on the same 96-well qRT-PCR plate. All primer-probe sets either contained a primer spanning an exon–exon boundary or primers spanning an intron. Expression levels of transcripts were normalized to 18S expression.

In vivo proliferation assay

In vivo proliferation was measured by a BrdU pulse 24 h before flow cytometric analysis. Each mouse received 0.8 mg BrdU injected i.p. on day 12 after tumor inoculation. TILs were isolated and surface staining was performed. After surface staining, cells were fixed and permeabilized using the Foxp3 staining kit (BD), according to manufacturer's protocol, and incubated with 100 µl PBS/DNase solution (300 µg/ml) for 30 min at 37°C. Cells were washed and incubated for 30 min at room temperature with anti-BrdU (FITC and Bu20a) and then washed with and resuspended in PBS.

In vitro stimulation assays

Tissue culture–treated 96-well round bottom plates were coated with anti-CD3ε (1 µg/ml; 2C11) in DPBS overnight at 4°C or for 2 h at 37°C. Cells were sorted into cold cDMEM media and put on ice as soon as the sort was finished. Cells were then pelleted, resuspended in 50 µl cDMEM, and incubated with soluble anti-CD28 (2 µg/ml; PV-1) for 10–12 h for a final volume of 100 µl. After stimulation, supernatants were removed for ELISA or bead-based immunoassay (LegendPlex), and cells were washed once with DPBS and resuspended in 15 µl of RNAlater Stabilization Solution (QIAGEN) or 300 µl of RLT buffer. Cells were stored at −80°C until RNA isolation was performed.

Protein quantification

Measurement of protein concentration was determined either by a standard ELISA or bead-based immunoassay (LEGENDplex; BioLegend) as indicated. ELISAs were performed according to the manufacturer's protocol (Ready-SET-Go ELISA; eBioscience) on supernatants from in vitro stimulations. Absorbance values were obtained at 450 nm using an Emax microplate reader (Molecular Devices), and IL-2 concentration was determined by standard curve. Protein concentration values were normalized to the number of sorted cells plated. LEGENDplex assays were performed according to the manufacturer's protocols.

Spectratype analysis and sequencing

Three mice were injected with 2×10^6 B16.SIY.dsRed tumor cells. 14 d later, tumors were harvested and specific $CD8^+$ TIL subpopulations were sorted into RLT buffer (QIAGEN) and immediately frozen. cDNA was synthesized from sorted cell populations and CDR3 regions were amplified by PCR with 21 different Vβ-5′ primers paired with a FAM-Cβ1.1 primer (Table S1). Three Vβ PCR reactions did not reach significant amplification for analysis and were removed from the analysis. For sequencing, Cβ-Vβ PCR products were purified using the

QIAquick PCR purification kit (QIAGEN) and sequenced at the University of Chicago Genomics Core Facility. Cβ-Vβ PCR products were analyzed by capillary electrophoresis at the University of Chicago Genomics core and CDR3 peaks were aligned using the Liz500 ladder. Spectratype graphs were displayed using the GeneiousR9 software (Kearse et al., 2012). To generate the frequency profile for each Vβ spectratype, the area under each peak was measured using Peak Studio (A. Fodor, University of North Carolina, Charlotte, NC). The HD (Currier and Robinson, 2001) was calculated between each Vβ spectratype from each $CD8^+$ spleen and TIL population within a given mouse. To determine significance between the HD from each comparison the HDs for each Vβ from 3 mice were averaged and a One-Way ANOVA with Dunn's correction for multiple comparisons was performed.

TCR transgenic T cell transfer experiments

Cell suspensions were generated from spleens and lymph nodes from congenic 2C/$Rag2^{-/-}$/CD45.1/2 and/or P14/$Rag2^{-/-}$/CD45.2 mice, and T cells were purified by $CD8^+$ negative selection (Miltenyi Biotec) over magnetic columns according to the manufacturer's protocol. TCR Tg T cells were washed with PBS and resuspended at a concentration of 10×10^6/ml, and 10^6 TCR Tg cells were adoptively transferred into CD45.1 tumor bearing mice by tail vein transfer in a volume of 0.1 ml. After the indicated times, 2C T cells and corresponding host $CD8^+$ T cells were sorted for in vitro stimulation.

In vitro cytotoxicity assay

Per individual experiment, 10 C57BL/6 mice were injected s.c. with 2×10^6 B16.SIY cells on both left and right flanks. On day 14, all 20 tumors were pooled and dissociated using the Tumor Dissociation kit (Miltenyi Biotec) following the manufacturer's protocol. Tumor cell suspensions were washed three to five times with PBS, and TILs were enriched for by Ficoll-Hypaque gradient centrifugation. TILs were stained, sorted and put directly on ice. TILs were titrated and added directly to a 96-well plate containing 50,000 P815 mastocytoma cells and 1 μg/ml anti-CD3. For a positive control, OT-I cells were isolated from OT-I/$Rag2^{-/-}$ mice and stimulated with plate-bound anti-CD3 (0.25 μg/ml), anti-CD28 (2 μg/ml) and 100 U/ml IL-2 for 2–3 d. For a negative control, P815 cells were cultured alone or cultured with naive $CD8^+$ T cells isolated from lymph nodes. After 12 h of incubation, cells were stained for Thy1, CD45, CD8α, Fixable Viability Dye 450 (eBioscience), and/or propidium iodide.

Gene expression analysis

Total RNA for the $CD8^+$ TIL subpopulations was isolated following the manufacturer's protocol (RNEasy Micro kit; QIAGEN) from sorted cells pooled from 10 mice. Samples were analyzed by the University of Chicago Genomics Facility using Illumina MouseRef8 microarray chips. Two experimental replicates were performed, and the results were $\log_2$ transformed and averaged. Probe sets that revealed a 1.5-fold difference abs($\log_2$ [ratio] > 1.5) relative to $CD8^+$4-1BB$^-$ LAG-3$^-$PD-1$^-$ cells were identified and used for subsequent analysis. The microarray data are available in the Gene Expression Omnibus database under accession no. GSE79919. For cross-study comparisons, $\log_2$-fold change values were extracted using the GEO2R online software from the hypofunctional $CD8^+$ TIL dataset GSE79858 (GSM2107353, GSM2107353, and GSM2107355 versus GSM2107350, GSM2107351, and GSM210732) and the $CD8^+$ T cell–exhausted dataset, GSE41870 (GSM1026819, GSM1026820, and GSM1026821 versus GSM1026786, GSM1026787, GSM1026788, and GSM1026789). Up-regulated genes showing a twofold difference were used for analysis. Multiple genes names from the GEO2R extracted data were identified and matched to gene names from the Illumina dataset. The rank-rank hypergeometric overlap (RRHO) analysis (Plaisier et al., 2010) was conducted through publicly available Rank-Rank Hypergeometric Overlap software (T. Graeber, University of California, Los Angeles, Los Angeles, CA) and the associated Bioconductor package RRHO (Rosenblatt and Stein, 2014).

Gene Ontology enrichment analysis

In a pairwise fashion, shared up-regulated genes (Table S3) were used as the input for the ClueGO software with the Cytoscape application (Shannon et al., 2003). Both the Biological Process and Immune System Process Gene Ontology Annotations were used for analysis. Only pathways with a Bonferroni step down correction P value > 0.01 were considered when generating pathway nodes. Nonredundant pathways with the greatest number of genes found within each node were used as examples in Fig. 6 A.

Antibody and FTY720 treatments

Mice were treated i.p. with 100 μg/mouse of anti–4-1BB (Bio-X-Cell; LOB12.3) antibody and/or 100 μg/mouse anti–LAG-3 (Bio-X-Cell; C9B7W). For tumor outgrowth experiments, mice were treated on day 7, 10, 13, and 16 after tumor inoculation. For ex vivo functional experiments, mice were treated on day 7, 10, and 13, and cells were sorted on day 14. For experiments blocking lymph node egress, 25 μg of FTY720 was given by gavage 1 d before first antibody treatment (day 6) and continued every day until endpoint on day 14.

Online supplemental material

Fig. S1 shows all spectratype graphs used in the analysis in Fig. 3 B. Fig. S2 shows $CD3^+$ T cells on day 14 after FTY720 administration. Fig. S3 contains statistical analysis of the cross-study comparison of gene expression profiles. Table S1 is a list of all Vβ primers and primer/probe sets. Tables S2 and S3 contain the grouped gene sets from Fig. 6 A. Table S4 shows the complete list of the identified pathways from each gene set in Fig. 6 A. Tables S1–S4 are available as Excel files.

ACKNOWLEDGMENTS

The authors thank Yesika Contreras for help in sample preparation, Dr. Marisa Alegre for helpful comments, and the Flow Cytometry core and Genomics facility of the University of Chicago Comprehensive Cancer Center.

This work was supported by National Institutes of Health grant R01 CA161005. The authors declare no conflicting financial interests.

Submitted: 4 April 2016
Revised: 8 September 2016
Accepted: 15 December 2016

REFERENCES

Ahmadzadeh, M., L.A. Johnson, B. Heemskerk, J.R. Wunderlich, M.E. Dudley, D.E. White, and S.A. Rosenberg. 2009. Tumor antigen-specific CD8 T cells infiltrating the tumor express high levels of PD-1 and are functionally impaired. *Blood.* 114:1537–1544. http://dx.doi.org/10.1182/blood-2008-12-195792

Baitsch, L., P. Baumgaertner, E. Devêvre, S.K. Raghav, A. Legat, L. Barba, S. Wieckowski, H. Bouzourene, B. Deplancke, P. Romero, et al. 2011. Exhaustion of tumor-specific $CD8^+$ T cells in metastases from melanoma patients. *J. Clin. Invest.* 121:2350–2360. http://dx.doi.org/10.1172/JCI46102

Baitsch, L., A. Legat, L. Barba, S.A. Fuertes Marraco, J.-P. Rivals, P. Baumgaertner, C. Christiansen-Jucht, H. Bouzourene, D. Rimoldi, H. Pircher, et al. 2012. Extended co-expression of inhibitory receptors by human CD8 T-cells depending on differentiation, antigen-specificity and anatomical localization. *PLoS One.* 7:e30852. http://dx.doi.org/10.1371/journal.pone.0030852

Blackburn, S.D., H. Shin, W.N. Haining, T. Zou, C.J. Workman, A. Polley, M.R. Betts, G.J. Freeman, D.A.A. Vignali, and E.J. Wherry. 2009. Coregulation of $CD8^+$ T cell exhaustion by multiple inhibitory receptors during chronic viral infection. *Nat. Immunol.* 10:29–37. http://dx.doi.org/10.1038/ni.1679

Brown, I.E., C. Blank, J. Kline, A.K. Kacha, and T.F. Gajewski. 2006. Homeostatic proliferation as an isolated variable reverses $CD8^+$ T cell anergy and promotes tumor rejection. *J. Immunol.* 177:4521–4529. http://dx.doi.org/10.4049/jimmunol.177.7.4521

Clouthier, D.L., A.C. Zhou, and T.H. Watts. 2014. Anti-GITR agonist therapy intrinsically enhances CD8 T cell responses to chronic lymphocytic choriomeningitis virus (LCMV), thereby circumventing LCMV-induced downregulation of costimulatory GITR ligand on APC. *J. Immunol.* 193:5033–5043. http://dx.doi.org/10.4049/jimmunol.1401002

Crawford, A., J.M. Angelosanto, C. Kao, T.A. Doering, P.M. Odorizzi, B.E. Barnett, and E.J. Wherry. 2014. Molecular and transcriptional basis of $CD4^+$ T cell dysfunction during chronic infection. *Immunity.* 40:289–302. http://dx.doi.org/10.1016/j.immuni.2014.01.005

Cunningham, C.R., A. Champhekar, M.V. Tullius, B.J. Dillon, A. Zhen, J.R. de la Fuente, J. Herskovitz, H. Elsaesser, L.M. Snell, E.B. Wilson, et al. 2016. Type I and Type II interferon coordinately regulate suppressive dendritic cell fate and function during viral persistence. *PLoS Pathog.* 12:e1005356. http://dx.doi.org/10.1371/journal.ppat.1005356

Currier, J.R., and M.A. Robinson. 2001. Spectratype/Immunoscope Analysis of the Expressed TCR Repertoire. John Wiley & Sons, Inc., Hoboken, NJ. 92544 pp. http://dx.doi.org/10.1002/0471142735.im1028s38

Diamond, M.S., M. Kinder, H. Matsushita, M. Mashayekhi, G.P. Dunn, J.M. Archambault, H. Lee, C.D. Arthur, J.M. White, U. Kalinke, et al. 2011. Type I interferon is selectively required by dendritic cells for immune rejection of tumors. *J. Exp. Med.* 208:1989–2003. http://dx.doi.org/10.1084/jem.20101158

Doering, T.A., A. Crawford, J.M. Angelosanto, M.A. Paley, C.G. Ziegler, and E.J. Wherry. 2012. Network analysis reveals centrally connected genes and pathways involved in $CD8^+$ T cell exhaustion versus memory. *Immunity.* 37:1130–1144. http://dx.doi.org/10.1016/j.immuni.2012.08.021

Evaristo, C., S. Spranger, S.E. Barnes, M.L. Miller, L.L. Molinero, F.L. Locke, T.F. Gajewski, and M.-L. Alegre. 2016. Cutting edge: engineering active IKKβ in T cells drives tumor rejection. *J. Immunol.* 196:2933–2938. http://dx.doi.org/10.4049/jimmunol.1501144

Fan, X., S.A. Quezada, M.A. Sepulveda, P. Sharma, and J.P. Allison. 2014. Engagement of the ICOS pathway markedly enhances efficacy of CTLA-4 blockade in cancer immunotherapy. *J. Exp. Med.* 211:715–725. http://dx.doi.org/10.1084/jem.20130590

Fourcade, J., Z. Sun, O. Pagliano, P. Guillaume, I.F. Luescher, C. Sander, J.M. Kirkwood, D. Olive, V. Kuchroo, and H.M. Zarour. 2012. $CD8^+$ T cells specific for tumor antigens can be rendered dysfunctional by the tumor microenvironment through upregulation of the inhibitory receptors BTLA and PD-1. *Cancer Res.* 72:887–896. http://dx.doi.org/10.1158/0008-5472.CAN-11-2637

Fridman, W.H., F. Pagès, C. Sautès-Fridman, and J. Galon. 2012. The immune contexture in human tumours: impact on clinical outcome. *Nat. Rev. Cancer.* 12:298–306. http://dx.doi.org/10.1038/nrc3245

Fuertes, M.B., A.K. Kacha, J. Kline, S.-R. Woo, D.M. Kranz, K.M. Murphy, and T.F. Gajewski. 2011. Host type I IFN signals are required for antitumor $CD8^+$ T cell responses through $CD8\alpha^+$ dendritic cells. *J. Exp. Med.* 208:2005–2016. http://dx.doi.org/10.1084/jem.20101159

Gajewski, T.F. 2007a. The expanding universe of regulatory T cell subsets in cancer. *Immunity.* 27:185–187. http://dx.doi.org/10.1016/j.immuni.2007.08.001

Gajewski, T.F. 2007b. Failure at the effector phase: immune barriers at the level of the melanoma tumor microenvironment. *Clin. Cancer Res.* 13:5256–5261. http://dx.doi.org/10.1158/1078-0432.CCR-07-0892

Gajewski, T.F., Y. Meng, C. Blank, I. Brown, A. Kacha, J. Kline, and H. Harlin. 2006. Immune resistance orchestrated by the tumor microenvironment. *Immunol. Rev.* 213:131–145. http://dx.doi.org/10.1111/j.1600-065X.2006.00442.x

Gajewski, T.F., H. Schreiber, and Y.-X. Fu. 2013. Innate and adaptive immune cells in the tumor microenvironment. *Nat. Immunol.* 14:1014–1022. http://dx.doi.org/10.1038/ni.2703

Goldszmid, R.S., A. Dzutsev, and G. Trinchieri. 2014. Host immune response to infection and cancer: unexpected commonalities. *Cell Host Microbe.* 15:295–305. http://dx.doi.org/10.1016/j.chom.2014.02.003

Gros, A., P.F. Robbins, X. Yao, Y.F. Li, S. Turcotte, E. Tran, J.R. Wunderlich, A. Mixon, S. Farid, M.E. Dudley, et al. 2014. PD-1 identifies the patient-specific $CD8^+$ tumor-reactive repertoire infiltrating human tumors. *J. Clin. Invest.* 124:2246–2259. http://dx.doi.org/10.1172/JCI73639

Halin, C., M.L. Scimone, R. Bonasio, J.-M. Gauguet, T.R. Mempel, E. Quackenbush, R.L. Proia, S. Mandala, and U.H. von Andrian. 2005. The S1P-analog FTY720 differentially modulates T-cell homing via HEV: T-cell-expressed S1P1 amplifies integrin activation in peripheral lymph nodes but not in Peyer patches. *Blood.* 106:1314–1322. http://dx.doi.org/10.1182/blood-2004-09-3687

Harlin, H., T.V. Kuna, A.C. Peterson, Y. Meng, and T.F. Gajewski. 2006. Tumor progression despite massive influx of activated $CD8^+$ T cells in a patient with malignant melanoma ascites. *Cancer Immunol. Immunother.* 55:1185–1197. http://dx.doi.org/10.1007/s00262-005-0118-2

Harlin, H., Y. Meng, A.C. Peterson, Y. Zha, M. Tretiakova, C. Slingluff, M. McKee, and T.F. Gajewski. 2009. Chemokine expression in melanoma metastases associated with $CD8^+$ T-cell recruitment. *Cancer Res.* 69:3077–3085. http://dx.doi.org/10.1158/0008-5472.CAN-08-2281

Hoelzinger, D.B., S.E. Smith, N. Mirza, A.L. Dominguez, S.Z. Manrique, and J. Lustgarten. 2010. Blockade of CCL1 inhibits T regulatory cell suppressive function enhancing tumor immunity without affecting T effector responses. *J. Immunol.* 184:6833–6842. http://dx.doi.org/10.4049/jimmunol.0904084

Jenkins, M.K., D.M. Pardoll, J. Mizuguchi, T.M. Chused, and R.H. Schwartz. 1987. Molecular events in the induction of a nonresponsive state in interleukin 2-producing helper T-lymphocyte clones. *Proc. Natl. Acad. Sci. USA.* 84:5409–5413. http://dx.doi.org/10.1073/pnas.84.15.5409

Johnston, R.J., L. Comps-Agrar, J. Hackney, X. Yu, M. Huseni, Y. Yang, S. Park, V. Javinal, H. Chiu, B. Irving, et al. 2014. The immunoreceptor TIGIT regulates antitumor and antiviral $CD8^+$ T cell effector function. *Cancer Cell.* 26:923–937. http://dx.doi.org/10.1016/j.ccell.2014.10.018

Joshi, N.S., W. Cui, A. Chandele, H.K. Lee, D.R. Urso, J. Hagman, L. Gapin, and S.M. Kaech. 2007. Inflammation directs memory precursor and short-lived effector $CD8^+$ T cell fates via the graded expression of T-bet transcription factor. *Immunity.* 27:281–295. http://dx.doi.org/10.1016/j.immuni.2007.07.010

Kaech, S.M., J.T. Tan, E.J. Wherry, B.T. Konieczny, C.D. Surh, and R. Ahmed. 2003. Selective expression of the interleukin 7 receptor identifies effector CD8 T cells that give rise to long-lived memory cells. *Nat. Immunol.* 4:1191–1198. http://dx.doi.org/10.1038/ni1009

Kearse, M., R. Moir, A. Wilson, S. Stones-Havas, M. Cheung, S. Sturrock, S. Buxton, A. Cooper, S. Markowitz, C. Duran, et al. 2012. Geneious Basic: an integrated and extendable desktop software platform for the organization and analysis of sequence data. *Bioinformatics.* 28:1647–1649. http://dx.doi.org/10.1093/bioinformatics/bts199

Kim, J.-O., H.W. Kim, K.-M. Baek, and C.-Y. Kang. 2003. NF-κB and AP-1 regulate activation-dependent CD137 (4-1BB) expression in T cells. *FEBS Lett.* 541:163–170. http://dx.doi.org/10.1016/S0014-5793(03)00326-0

Kline, J., L. Zhang, L. Battaglia, K.S. Cohen, and T.F. Gajewski. 2012. Cellular and molecular requirements for rejection of B16 melanoma in the setting of regulatory T cell depletion and homeostatic proliferation. *J. Immunol.* 188:2630–2642. http://dx.doi.org/10.4049/jimmunol.1100845

Kuchroo, V.K., A.C. Anderson, and C. Petrovas. 2014. Coinhibitory receptors and CD8 T cell exhaustion in chronic infections. *Curr. Opin. HIV AIDS.* 9:439–445. http://dx.doi.org/10.1097/COH.0000000000000088

Larkin, J., F.S. Hodi, and J.D. Wolchok. 2015. Combined Nivolumab and Ipilimumab or monotherapy in untreated melanoma. *N. Engl. J. Med.* 373:1270–1271. http://dx.doi.org/10.1056/NEJMoa1504030

Li, S., T. Miao, M. Sebastian, P. Bhullar, E. Ghaffari, M. Liu, A.L.J. Symonds, and P. Wang. 2012. The transcription factors Egr2 and Egr3 are essential for the control of inflammation and antigen-induced proliferation of B and T cells. *Immunity.* 37:685–696. http://dx.doi.org/10.1016/j.immuni.2012.08.001

Martinez, G.J., R.M. Pereira, T. Äijö, E.Y. Kim, F. Marangoni, M.E. Pipkin, S. Togher, V. Heissmeyer, Y.C. Zhang, S. Crotty, et al. 2015. The transcription factor NFAT promotes exhaustion of activated $CD8^+$ T cells. *Immunity.* 42:265–278. http://dx.doi.org/10.1016/j.immuni.2015.01.006

Odorizzi, P.M., K.E. Pauken, M.A. Paley, A. Sharpe, and E.J. Wherry. 2015. Genetic absence of PD-1 promotes accumulation of terminally differentiated exhausted $CD8^+$ T cells. *J. Exp. Med.* 212:1125–1137. http://dx.doi.org/10.1084/jem.20142237

Palazón, A., I. Martínez-Forero, A. Teijeira, A. Morales-Kastresana, C. Alfaro, M.F. Sanmamed, J.L. Perez-Gracia, I. Peñuelas, S. Hervás-Stubbs, A. Rouzaut, et al. 2012. The HIF-1α hypoxia response in tumor-infiltrating T lymphocytes induces functional CD137 (4-1BB) for immunotherapy. *Cancer Discov.* 2:608–623. http://dx.doi.org/10.1158/2159-8290.CD-11-0314

Pardoll, D.M. 2012. The blockade of immune checkpoints in cancer immunotherapy. *Nat. Rev. Cancer.* 12:252–264. http://dx.doi.org/10.1038/nrc3239

Pauken, K.E., and E.J. Wherry. 2015. Overcoming T cell exhaustion in infection and cancer. *Trends Immunol.* 36:265–276. http://dx.doi.org/10.1016/j.it.2015.02.008

Pearce, E.L., M.C. Poffenberger, C.H. Chang, and R.G. Jones. 2013. Fueling immunity: insights into metabolism and lymphocyte function. *Science.* 342:1242454. http://dx.doi.org/10.1126/science.1242454

Plaisier, S.B., R. Taschereau, J.A. Wong, and T.G. Graeber. 2010. Rank-rank hypergeometric overlap: identification of statistically significant overlap between gene-expression signatures. *Nucleic Acids Res.* 38:e169–e169. http://dx.doi.org/10.1093/nar/gkq636

Rosenblatt, J.D., and J.L. Stein. 2014. RRHO: Test overlap using the Rank-Rank Hypergeometric test. R package. https://bioconductor.riken.jp/packages/3.1/bioc/html/RRHO.html.

Safford, M., S. Collins, M.A. Lutz, A. Allen, C.-T. Huang, J. Kowalski, A. Blackford, M.R. Horton, C. Drake, R.H. Schwartz, and J.D. Powell. 2005. Egr-2 and Egr-3 are negative regulators of T cell activation. *Nat. Immunol.* 6:472–480. http://dx.doi.org/10.1038/ni1193

Sarkar, S., V. Kalia, W.N. Haining, B.T. Konieczny, S. Subramaniam, and R. Ahmed. 2008. Functional and genomic profiling of effector CD8 T cell subsets with distinct memory fates. *J. Exp. Med.* 205:625–640. http://dx.doi.org/10.1084/jem.20071641

Sarris, M., K.G. Andersen, F. Randow, L. Mayr, and A.G. Betz. 2008. Neuropilin-1 expression on regulatory T cells enhances their interactions with dendritic cells during antigen recognition. *Immunity.* 28:402–413. http://dx.doi.org/10.1016/j.immuni.2008.01.012

Schietinger, A., and P.D. Greenberg. 2014. Tolerance and exhaustion: defining mechanisms of T cell dysfunction. *Trends Immunol.* 35:51–60. http://dx.doi.org/10.1016/j.it.2013.10.001

Schietinger, A., M. Philip, V.E. Krisnawan, E.Y. Chiu, J.J. Delrow, R.S. Basom, P. Lauer, D.G. Brockstedt, S.E. Knoblaugh, G.J. Hämmerling, et al. 2016. Tumor-specific T cell dysfunction is a dynamic antigen-driven differentiation program initiated early during tumorigenesis. *Immunity.* 45:389–401. http://dx.doi.org/10.1016/j.immuni.2016.07.011

Schwartz, R.H. 2003. T cell anergy. *Annu. Rev. Immunol.* 21:305–334. http://dx.doi.org/10.1146/annurev.immunol.21.120601.141110

Schwartz, R.H., D.L. Mueller, M.K. Jenkins, and H. Quill. 1989. T-cell clonal anergy. *Cold Spring Harb. Symp. Quant. Biol.* 54:605–610. http://dx.doi.org/10.1101/SQB.1989.054.01.072

Shannon, P., A. Markiel, O. Ozier, N.S. Baliga, J.T. Wang, D. Ramage, N. Amin, B. Schwikowski, and T. Ideker. 2003. Cytoscape: a software environment for integrated models of biomolecular interaction networks. *Genome Res.* 13:2498–2504. http://dx.doi.org/10.1101/gr.1239303

Snell, L.M., and D.G. Brooks. 2015. New insights into type I interferon and the immunopathogenesis of persistent viral infections. *Curr. Opin. Immunol.* 34:91–98. http://dx.doi.org/10.1016/j.coi.2015.03.002

Spiotto, M.T., P. Yu, D.A. Rowley, M.I. Nishimura, S.C. Meredith, T.F. Gajewski, Y.-X. Fu, and H. Schreiber. 2002. Increasing tumor antigen expression overcomes "ignorance" to solid tumors via crosspresentation by bone marrow-derived stromal cells. *Immunity.* 17:737–747. http://dx.doi.org/10.1016/S1074-7613(02)00480-6

Spranger, S., R.M. Spaapen, Y. Zha, J. Williams, Y. Meng, T.T. Ha, and T.F. Gajewski. 2013. Up-regulation of PD-L1, IDO, and T(regs) in the melanoma tumor microenvironment is driven by CD8(+) T cells. *Sci. Transl. Med.* 5:200ra116.

Spranger, S., H.K. Koblish, B. Horton, P.A. Scherle, R. Newton, and T.F. Gajewski. 2014. Mechanism of tumor rejection with doublets of CTLA-4, PD-1/PD-L1, or IDO blockade involves restored IL-2 production and proliferation of $CD8^+$ T cells directly within the tumor microenvironment. *J. Immunother. Cancer.* 2:3.

Sumitomo, S., K. Fujio, T. Okamura, and K. Yamamoto. 2013. Egr2 and Egr3 are the unique regulators for systemic autoimmunity. *JAK-STAT.* 2:e23952. http://dx.doi.org/10.4161/jkst.23952

Tumeh, P.C., C.L. Harview, J.H. Yearley, I.P. Shintaku, E.J.M. Taylor, L. Robert, B. Chmielowski, M. Spasic, G. Henry, V. Ciobanu, et al. 2014. PD-1

blockade induces responses by inhibiting adaptive immune resistance. *Nature.* 515:568–571. http://dx.doi.org/10.1038/nature13954

Twyman-Saint Victor, C., A.J. Rech, A. Maity, R. Rengan, K.E. Pauken, E. Stelekati, J.L. Benci, B. Xu, H. Dada, P.M. Odorizzi, et al. 2015. Radiation and dual checkpoint blockade activate non-redundant immune mechanisms in cancer. *Nature.* 520:373–377. http://dx.doi.org/10.1038/nature14292

Vesely, M.D., M.H. Kershaw, R.D. Schreiber, and M.J. Smyth. 2011. Natural innate and adaptive immunity to cancer. *Annu. Rev. Immunol.* 29:235–271. http://dx.doi.org/10.1146/annurev-immunol-031210-101324

Waugh, K.A., S.M. Leach, B.L. Moore, T.C. Bruno, J.D. Buhrman, and J.E. Slansky. 2016. Molecular profile of tumor-specific $CD8^+$ T cell hypofunction in a transplantable murine cancer model. *J. Immunol.* 197:1477–1488. http://dx.doi.org/10.4049/jimmunol.1600589

Wherry, E.J., and M. Kurachi. 2015. Molecular and cellular insights into T cell exhaustion. *Nat. Rev. Immunol.* 15:486–499. http://dx.doi.org/10.1038/nri3862

Wherry, E.J., S.-J. Ha, S.M. Kaech, W.N. Haining, S. Sarkar, V. Kalia, S. Subramaniam, J.N. Blattman, D.L. Barber, and R. Ahmed. 2007. Molecular signature of CD8+ T cell exhaustion during chronic viral infection. *Immunity.* 27:670–684. http://dx.doi.org/10.1016/j.immuni.2007.09.006

Wu, X., H. Zhang, Q. Xing, J. Cui, J. Li, Y. Li, Y. Tan, and S. Wang. 2014. PD-1^+ $CD8^+$ T cells are exhausted in tumours and functional in draining lymph nodes of colorectal cancer patients. *Br. J. Cancer.* 111:1391–1399. http://dx.doi.org/10.1038/bjc.2014.416

Zajac, A.J., J.N. Blattman, K. Murali-Krishna, D.J. Sourdive, M. Suresh, J.D. Altman, and R. Ahmed. 1998. Viral immune evasion due to persistence of activated T cells without effector function. *J. Exp. Med.* 188:2205–2213. http://dx.doi.org/10.1084/jem.188.12.2205

Zha, Y., R. Marks, A.W. Ho, A.C. Peterson, S. Janardhan, I. Brown, K. Praveen, S. Stang, J.C. Stone, and T.F. Gajewski. 2006. T cell anergy is reversed by active Ras and is regulated by diacylglycerol kinase-alpha. *Nat. Immunol.* 7:1166–1173. http://dx.doi.org/10.1038/ni1394

Zhang, L., T.F. Gajewski, and J. Kline. 2009. PD-1/PD-L1 interactions inhibit antitumor immune responses in a murine acute myeloid leukemia model. *Blood.* 114:1545–1552. http://dx.doi.org/10.1182/blood-2009-03-206672

Zheng, Y., Y. Zha, G. Driessens, F. Locke, and T.F. Gajewski. 2012. Transcriptional regulator early growth response gene 2 (Egr2) is required for T cell anergy in vitro and in vivo. *J. Exp. Med.* 209:2157–2163. http://dx.doi.org/10.1084/jem.20120342

Zheng, Y., Y. Zha, R.M. Spaapen, R. Mathew, K. Barr, A. Bendelac, and T.F. Gajewski. 2013. Egr2-dependent gene expression profiling and ChIP-Seq reveal novel biologic targets in T cell anergy. *Mol. Immunol.* 55:283–291. http://dx.doi.org/10.1016/j.molimm.2013.03.006